J. Fluid Mech. (1999), *vol.* 399, *pp.* 151–204. Printed in the United Kingdom

Evaporation of acoustically levitated droplets

By A. L. YARIN[1], G. BRENN[2]†, O. KASTNER[2], D. RENSINK[2] AND C. TROPEA[3]

[1] Faculty of Mechanical Engineering, Technion-Israel Institute of Technology, Haifa 32000, Israel

[2] Lehrstuhl für Strömungsmechanik (LSTM), University of Erlangen-Nürnberg, Cauerstraße 4, D-91058 Erlangen, Germany

[3] Fachgebiet Strömungslehre und Aerodynamik (SLA), Technical University of Darmstadt, Petersenstraße 30, D-64287 Darmstadt, Germany

(Received 2 November 1998 and in revised form 21 April 1999)

The rate of heat and mass transfer at the surface of acoustically levitated pure liquid droplets is predicted theoretically for the case where an acoustic boundary layer appears near the droplet surface resulting in an acoustic streaming. The theory is based on the computation of the acoustic field and squeezed droplet shape by means of the boundary element method developed in Yarin, Pfaffenlehner & Tropea (1998). Given the acoustic field around the levitated droplet, the acoustic streaming near the droplet surface was calculated. This allowed calculation of the Sherwood and Nusselt number distributions over the droplet surface, as well as their average values. Then, the mass balance was used to calculate the evolution of the equivalent droplet radius in time.

The theory is applicable to droplets of arbitrary size relative to the sound wavelength λ, including those of the order of λ, when the compressible character of the gas flow is important. Also, the deformation of the droplets by the acoustic field is accounted for, as well as a displacement of the droplet centre from the pressure node. The effect of the internal circulation of liquid in the droplet sustained by the acoustic streaming in the gas is estimated. The distribution of the time-average heat and mass transfer rate over the droplet surface is found to have a maximum at the droplet equator and minima at its poles. The time and surface average of the Sherwood number was shown to be described by the expression $Sh = KB/\sqrt{\omega\mathscr{D}_0}$, where $B = A_{0e}/(\rho_0 c_0)$ is a scale of the velocity in the sound wave (A_{0e} is the amplitude of the incident sound wave, ρ_0 is the unperturbed air density, c_0 is the sound velocity in air, ω is the angular frequency in the ultrasonic range, $\mathscr{D}_0$ is the mass diffusion coefficient of liquid vapour in air, which should be replaced by the thermal diffusivity of air in the computation of the Nusselt number). The coefficient K depends on the governing parameters (the acoustic field, the liquid properties), as well as on the current equivalent droplet radius a.

For small spherical droplets with $a \ll \lambda$, $K = (45/4\pi)^{1/2} = 1.89$, if A_{0e} is found from the sound pressure level (SPL) defined using A_{0e}. On the other hand, if A_{0e} is found from the same value of the SPL, but defined using the root-mean-square pressure amplitude ($p_{rms} = A_{0e}/\sqrt{2}$), then $Sh = K_{rms}B_{rms}/\sqrt{\omega\mathscr{D}_0}$, with $B_{rms} = \sqrt{2}B$ and $K_{rms} = K/\sqrt{2} = 1.336$. For large droplets squeezed significantly by the acoustic field, K appears always to be greater than 1.89. The evolution of an evaporating droplet in time is predicted and compared with the present experiments and existing data from the literature. The agreement is found to be rather good.

We also study and discuss the effect of an additional blowing (a gas jet impinging on a droplet) on the evaporation rate, as well as the enrichment of gas at the

† Author to whom correspondence should be addressed.

outer boundary of the acoustic bondary layer by liquid vapour. We show that, even at relatively high rates of blowing, the droplet evaporation is still governed by the acoustic streaming in the relatively strong acoustic fields we use. This makes it impossible to study forced convective heat and mass transfer under the present conditions using droplets levitated in strong acoustic fields.

1. Introduction

The acoustic levitation of droplets is a valuable tool for studying heat and mass transfer at the droplet surface because it allows steady droplet positioning. However, acoustic levitation results in an acoustic streaming near the droplet surface (see e.g. the recent review by Riley 1997) which may affect the heat and mass transfer rate.

In spite of the fact that heat and mass transfer at the droplet surface in a stagnant gas or a gas flow without an acoustic field has received significant attention for a long time and many theoretical and experimental results are available (see, for example, Maisel & Sherwood 1950; Ranz & Marshall 1952*a*, *b*; and Bird, Stewart & Lightfoot 1960), the acoustic-driven counterparts of these processes are much less understood. Some experimental data on sublimation and evaporation of a levitated sample (or a sample fixed in the acoustic field), as well as on heat transfer at its surface can be found in Burdukov & Nakoryakov (1965*a*, *b*, 1967), Richardson (1967), Larsen & Jensen (1978), Seaver, Galloway and Manuccia (1989), Seaver & Peele (1990), Gopinath & Mills (1993) and Tian & Apfel (1996). These works deal with droplets as well as with solid spheres and cylinders.

A key element of the heat and mass transfer processes at the surface of levitated droplets is the acoustic streaming, first recognized by Rayleigh (1883) in regard of Kundt's dust patterns in a channel. Schlichting (1932, 1979) considered the problem of an oscillating cylinder in a fluid or gas at rest, which is closely related to the subject of the present work. He extended the method of successive approximations dating back to Rayleigh (pp. 410 and 428–430 in Schlichting 1979), which allowed him to calculate the acoustic streaming near an oscillating cylinder and to explain the experimental findings of Andrade (1931). Another modification of the method of successive approximations has been recently reviewed by Riley (1997) who denotes the acoustic streaming of this type as Type (a), to distinguish it from the acoustic streaming due to sound attenuation in the bulk, which he denotes as Type (b) or 'quartz wind'. A different terminology is used in other sources, e.g. Krasilnikov & Krylov (1984) refer to the acoustic streaming we are dealing with (Type a) as the Schlichting-type acoustic streaming.

Burdukov & Nakoryakov (1965*b*) and Lee & Wang (1989, 1990) applied perturbation methods related to those of Rayleigh and Schlichting to calculate the acoustic streaming near an extremely small rigid sphere positioned in a standing plane sound wave. Burdukov & Nakoryakov (1965*b*) also calculated the mass transfer rate at the sphere surface and conducted an experiment to verify their theory. Their final result includes an erroneous multiplier, which is discussed in § 7 below, due to which their comparison with the experiment (which also does not correspond to the validity range of their theory) seems to be inconclusive.

In the present work we are interested in the range where the Strouhal and Reynolds numbers based on the field parameters are large (see (2.1) to (2.4) below), whereas the Prandtl and Schmidt numbers are of the order one. Also the streaming Reynolds

number (see (5.20) below) is of the order one. Under such conditions the acoustic streaming dominates the mass transfer rate at the droplet surface (Burdukov & Nakoryakov 1965*b*; Richardson 1967; Larsen & Jensen 1978; Riley 1997 and references therein).

The theory of Burdukov & Nakoryakov (1965*b*) is based on several main assumptions. One of them is very restrictive: their assumption that the levitated particle is a sphere does not fit well the situation in the acoustic levitator where droplets are squeezed by the acoustic pressure and acquire an oblate shape (here and hereinafter we have in mind levitation of large liquid droplets in a gas host under the gravitational field; see e.g. Yarin, Pfaffenlehner & Tropea 1998, referred to as YPT hereafter). The assumption of Burdukov & Nakoryakov (1965*b*) that the droplet radius is much less than the sound wavelength (and, as a result, the gas flow is effectively incompressible) does not hold in many practically important situations. For example, it does not hold in any case studied theoretically and experimentally in YPT.

The main goal of the present work is to remove these restrictive assumptions and to predict the heat and mass transfer rates at the surface of oblate pure liquid droplets levitated acoustically and displaced below the pressure node. Also the restriction on the sound wavelength is removed allowing consideration of the compressible acoustic streaming and its effect on the heat and mass transfer. We shall also study experimentally and theoretically the effect of blowing on a droplet.

In § 2 some physical estimates are given which allow a reasonable simplification of the problem. In § 3 the equations of the compressible acoustic boundary layer in the gas near the droplet surface are posed. Their solution leading to the acoustic streaming is obtained in § 4. In § 5 we show how the general result for the acoustic streaming reduces to the incompressible case of the acoustic streaming near a small sphere positioned at the pressure node. Heat and mass transfer at the surface of the acoustically levitated droplet are treated in § 6, where the dependences of the Sherwood and Nusselt numbers on the governing parameters are obtained (some details of the calculations are given in Appendix A). The incompressible limit for the Sherwood and Nusselt numbers in the case of a small spherical particle positioned at the pressure node is obtained from the general result of § 6 in § 7. In § 8 we calculate the vapour concentration at the droplet surface, as well as the droplet temperature. We also calculate the vapour concentration at the outer boundary of the diffusion boundary layer. In § 9 we rearrange the main results of the present work to the form of equations (9.1) to (9.5) and (9.14). We implement them numerically, compare the results with the results of the experiment also described in § 9 and present a discussion. One of the outcomes is that blowing mainly affects the evaporation rate via variation of the vapour concentration at the outer boundary of the acoustic boundary layer. Even at relatively high rates of blowing, the evaporation under the present conditions is still governed by the acoustic mechanism which makes it impossible to study forced convective heat and mass transfer using droplets levitated acoustically in relatively strong fields. Conclusions are given in § 10. Appendix B contains a calculation of the internal circulation in a levitated droplet driven by the acoustic streaming in the gas and estimates its effect on the evaporation rate.

2. Physical estimates and resulting simplifying assumptions

In the present section we introduce a number of assumptions, which will be relevant for simplifications of the further theoretical development. These assumptions hold in

the parameter range involved in the present work, which allows one to consider them simply as relevant physical estimates.

(i) We assume that the incident standing plane acoustic wave does not change due to the increase of concentration of an evaporating component. In the case of heat removal from a heated particle this assumption is valid only if the temperature differences are small and the free convection is excluded (say, in weightlessness). Otherwise the levitation force may be significantly altered and the particle may even jump out of the levitator (Leung & Wang 1985; Zevenbergen *et al.* 1998). Another source of variation of the incident acoustic wave may be related to self-tuning of the levitator due to a decrease of the droplet size and changes in the drop shape in the course of evaporation. This results in an increase of the amplitude of the incident acoustic wave (at a fixed frequency). This phenomenon is accounted for in the present work (see § 9.3).

(ii) We also assume that droplets are practically impenetrable to the sound wave since fluids of interest have much larger values of the acoustic impedance than that of air (see e.g. Shi & Apfel 1995 and YPT).

(iii) Throughout the main body of the paper we neglect any flow inside a levitated droplet, considering its fluid to be at rest. This assumption will be supported *a posteriori* in Appendix B. There the internal circulation arising in the levitated droplet due to liquid entrainment by the acoustic streaming in the gas will be calculated in detail and compared with experimental data. The corresponding estimates also presented in Appendix B will show that the effect of the circulation on the evaporation rate is negligibly small in the parameter range involved. An estimate of a possible Marangoni convection within the liquid in the case of heat removal from a warm droplet is also given in Appendix B.

(iv) Kinematic viscosity, thermal diffusivity and diffusion coefficients of an evaporating component are assumed to be independent of the mixture composition.

(v) The Reynolds number based on the sound frequency

$$Re = \frac{\omega a^2}{\nu_0} \tag{2.1}$$

is assumed to be much larger than unity ($Re \gg 1$). Here ω is the angular frequency of the incident sound wave (corresponding to the ultrasonic range), a is an unperturbed volume-equivalent droplet radius, and ν_0 is the unperturbed kinematic viscosity of the gas surrounding the droplet. Typical values of the parameters corresponding to the values given in YPT are as follows: $\omega = 2\pi \times 56000\,\mathrm{Hz}$, $a \sim 10^{-1}\,\mathrm{cm}$, and $\nu_0 \sim 0.15\,\mathrm{cm^2\,s^{-1}}$. For these values $Re = 2.3 \times 10^4 \gg 1$, and the assumption definitely holds.

(vi) Denote the effective pressure amplitude of the incident acoustic field A_{0e}, and introduce

$$B = \frac{A_{0e}}{\rho_0 c_0}, \tag{2.2}$$

which is a velocity scale based on the amplitude (actually B is the gas particle velocity amplitude), ρ_0 is the unperturbed gas density, and c_0 is the sound velocity.

We assume that the reciprocal Strouhal number

$$S^{-1} = \frac{B}{\omega a} \ll 1, \tag{2.3}$$

which is identical to the assumption used by Schlichting (1932, 1979) for a scale of

gas particle displacement s:

$$s = \frac{B}{\omega} \ll a. \tag{2.4}$$

Therefore in our case the Strouhal number S is assumed to be large. For the high values of Re and S we are dealing with, the acoustic boundary layer (the Stokes layer) is formed in the gas near the droplet surface.

Note that

$$\frac{B}{\omega a} = \frac{A_{0e}}{\rho_0 c_0^2}\frac{1}{\Omega}, \quad \Omega = \frac{\omega a}{c_0}. \tag{2.5a,b}$$

The value of the pressure amplitude corresponding to the sound pressure level (SPL) of, say, 160 dB is about $A_{0e} = 2 \times 10^4\,\mathrm{dyne\,cm^{-2}}$ (cf. (9.12) below). Given $\rho_0 = 1.18 \times 10^{-3}\,\mathrm{g\,cm^{-3}}$ and $c_0 = 3.4 \times 10^4\,\mathrm{cm\,s^{-1}}$, the value of the dimensionless pressure amplitude $A_{0e}/(\rho_0 c_0^2) = O(10^{-2})$, like in YPT, whereas $\Omega \sim 1$, and thus via (2.5a) condition (2.3) always holds. Therefore in our case $B/(\omega a) \sim 10^{-2}$, and we can also apply the method of successive approximations based on (2.3). Note that for $a \sim 10^{-1}$ cm and $\omega = 2\pi \times 56000$ Hz we obtain $B \approx 352\,\mathrm{cm\,s^{-1}}$.

(vii) We assume that the Stefan flow at the droplet surface arising due to evaporation is negligible and impose the condition of zero normal velocity there. This assumption is not restrictive and may be removed if necessary (which is expected to yield only minor changes).

It is emphasized that we do not assume anything about the droplet shape (except that it is axisymmetric) or displacement from the pressure node. We also do not impose any restrictions on the value of $\Omega = \omega a/c_0 = ka$ (with $k = 2\pi/\lambda$ as a sound wavenumber), whereas Burdukov & Nakoryakov (1965b) assumed $\Omega \ll 1$. The values of $\Omega \sim 1$ correspond to levitated droplets studied theoretically and experimentally in YPT.

3. Compressible acoustic boundary layer in the gas near the droplet surface

The equations of the unsteady compressible boundary layer in the gas near the surface of a body of revolution (a droplet) take the form (Schlichting 1979)

$$\frac{\partial \rho r}{\partial t} + \frac{\partial \rho u r}{\partial x} + \frac{\partial \rho v r}{\partial y} = 0, \tag{3.1a}$$

$$\rho\left(\frac{\partial u}{\partial t} + u\frac{\partial u}{\partial x} + v\frac{\partial u}{\partial y}\right) = \rho\left(\frac{\partial U}{\partial t} + U\frac{\partial U}{\partial x}\right) + \frac{\partial}{\partial y}\left(\mu\frac{\partial u}{\partial y}\right). \tag{3.1b}$$

Here x is the arclength of the droplet generatrix from the bottom O_1 (see figure 1); y is the coordinate normal to x ($y = 0$ at the droplet surface); u and v are the velocity components in the x- and y-directions; ρ and μ are the gas density and viscosity, respectively.

The droplet shape (given by two coordinates $r(x)$ and $z(x)$, see figure 1) is considered to be known, since it was calculated in YPT. The velocity distribution U at the outer boundary of the boundary layer is also known (we discuss it in more detail below in this section).

The pressure p in the gas may be represented as a sum of an unperturbed pressure p_0 and perturbations produced by the incident and scattered acoustic fields p_i' and p_s'

$$p = p_0 + p_i' + p_s'. \tag{3.2}$$

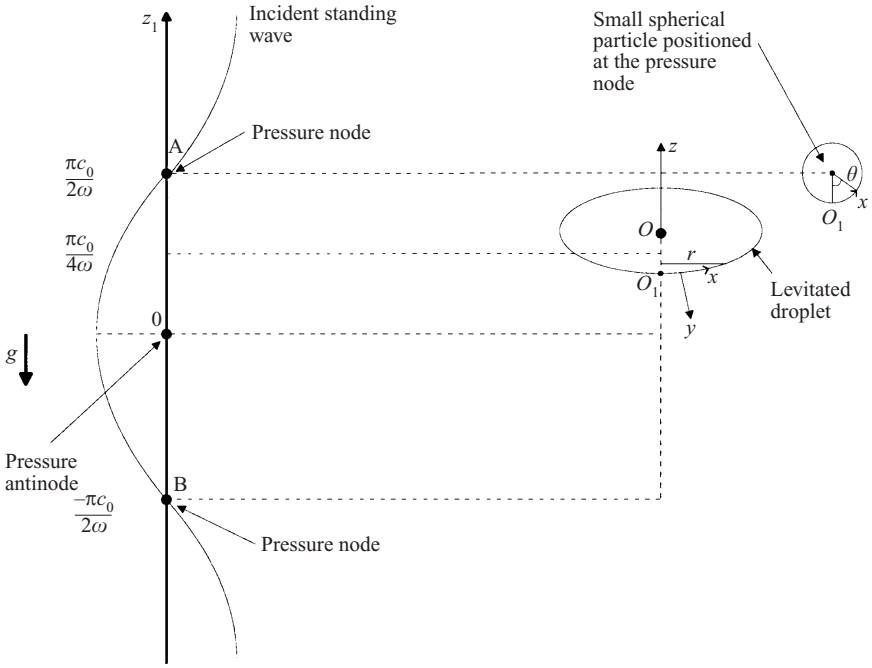

FIGURE 1. Sketch of the incident acoustic wave and a levitated droplet, with the frames of reference.

According to YPT, in the acoustic levitator

$$p_i' = A_{0e}\mathrm{e}^{-\mathrm{i}\omega t}\cos\frac{\omega z_1}{c_0}, \qquad p_s' = A_{0e}\mathrm{e}^{-\mathrm{i}\omega t}p_s, \tag{3.3a,b}$$

where t is time, i is the imaginary unit, and the factor p_s satisfies the Helmholtz equation

$$\Delta p_s + \left(\frac{\omega}{c_0}\right)^2 p_s = 0. \tag{3.4}$$

Note also that $z_1 = z + L$, where L is a displacement of a probe (or an imaginary) spherical particle from the pressure antinode (see YPT). In YPT equation (3.4) was solved using the boundary element method, which allowed determination of the acoustic field scattered from an oblate droplet displaced from the pressure node. Therefore we can consider the real and imaginary parts of $p_s = p_{sr}(x) + \mathrm{i}p_{si}(x)$ to be known at the droplet surface and according to (3.2) and (3.3a) the real part of the pressure distribution over the droplet surface is given as

$$p = p_0 + p' = p_0 + A_{0e}\cos\omega t\left(\cos\frac{\omega z_1}{c_0} + p_{sr}\right) + A_{0e}\sin\omega t\, p_{si}, \tag{3.5}$$

where $p' = p_i' + p_s'$.

Primarily the velocity of the gas in the acoustic field $\boldsymbol{v}'$ is related to the pressure perturbation according to

$$\boldsymbol{v}' = \nabla\left(-\frac{1}{\rho_0}\int_0^t p'\mathrm{d}t\right). \tag{3.6}$$

Equations (3.5) and (3.6) allow determination of the velocity distribution U over the

outer boundary of the acoustic boundary layer entering equation (3.1*b*) as

$$U = \frac{A_{0e}}{\omega\rho_0}\left[\cos\omega t\,\frac{\partial p_{si}}{\partial x} + \sin\omega t\,\left(\sin\frac{\omega z_1}{c_0}\,\frac{\omega}{c_0}\frac{\partial z}{\partial x} - \frac{\partial p_{sr}}{\partial x}\right)\right]. \tag{3.7}$$

To simplify the continuity equation (3.1*a*), we note that the following estimates hold:

$$u \sim B, \qquad U \sim B, \tag{3.8a, b}$$

where B is given by (2.2).

The thickness of the acoustic boundary layer (the inner streaming layer) is of the order of $\delta = (2\nu_0/\omega)^{1/2}$ (Schlichting 1932, 1979). The scale of x is a, whereas the scale of y in the boundary layer is δ. Since in the boundary layer (either incompressible or compressible) $\partial u/\partial x$ should be of the order of $\partial v/\partial y$, we obtain with the help of (3.8*a*)

$$v \sim \frac{B}{a}\left(\frac{2\nu_0}{\omega}\right)^{1/2}. \tag{3.9}$$

In the acoustic field (Landau & Lifshitz 1959, § 64)

$$\rho' = \frac{p'}{c_0^2} \tag{3.10}$$

and thus due to (3.3)

$$\rho' \sim \frac{A_{0e}}{c_0^2}, \tag{3.11}$$

where ρ' is the density perturbation. Considering the second term of the continuity equation (3.1*a*) and accounting for $\rho = \rho_0 + \rho'$, we obtain

$$\frac{\partial \rho u r}{\partial x} = \rho\frac{\partial u r}{\partial x} + u r\frac{\partial \rho'}{\partial x}\,, \tag{3.12}$$

where $x \sim a$ and $r \sim a$. Thus due to (3.8*a*)

$$\rho\frac{\partial u r}{\partial x} \sim \rho_0 B, \qquad u r\frac{\partial \rho'}{\partial x} \sim B\frac{A_{0e}}{c_0^2}. \tag{3.13}$$

Therefore

$$\frac{u r\partial\rho'/\partial x}{\rho\partial u r/\partial x} = \frac{A_{0e}}{\rho_0 c_0^2} \sim 10^{-2} \tag{3.14}$$

and we can neglect the term $u r\partial\rho'/\partial x$ relative to $\rho\partial u r/\partial x$.

Similarly, for the third term of the continuity equation (3.1*a*)

$$\frac{\partial \rho v r}{\partial y} = \rho\frac{\partial v r}{\partial y} + v r\frac{\partial \rho'}{\partial y} \tag{3.15}$$

we find that, for $y \sim \delta = (2\nu_0/\omega)^{1/2}$ and v estimated as in (3.9), one can neglect $v r\partial\rho'/\partial y$ relative to $\rho\partial v r/\partial y$.

As a result, the continuity equation (3.1*a*) is reduced in the leading order to

$$\frac{\partial u r}{\partial x} + \frac{\partial v r}{\partial y} = -\frac{r}{\rho_0}\frac{\partial \rho'}{\partial t}. \tag{3.16}$$

Substituting (3.10) and (3.5) in (3.16), we obtain the continuity equation in the

final form

$$\frac{\partial ur}{\partial x}+\frac{\partial vr}{\partial y}=-r\frac{\omega}{c_0}B\left[-\left(\cos\frac{\omega z_1}{c_0}+p_{sr}\right)\sin\omega t+p_{si}\cos\omega t\right]. \tag{3.17}$$

To rearrange the momentum equation (3.1*b*), we assume the viscosity–temperature dependence in the power-law form

$$\frac{\mu}{\mu_0}=\left(\frac{T}{T_0}\right)^n, \tag{3.18}$$

where the subscript zero denotes the unperturbed values, which in the linear approximation reduces to

$$\mu=\mu_0\left(1+n\frac{T'}{T_0}\right), \tag{3.19}$$

where T' is the temperature perturbation.

From the equation of state $p/\rho=R_sT$ (R_s is the specific gas constant) it follows that in the linear acoustic approximation

$$\frac{p'}{p_0}-\frac{\rho'}{\rho_0}=\frac{T'}{T_0}. \tag{3.20}$$

We assume the situation to be almost adiabatic over the boundary layer thickness, neglecting at the moment a possible effect on the boundary layer of the latent heat of evaporation, or heating/cooling from the droplet side. In this case the adiabatic law $p\rho^{-\gamma}=p_0\rho_0^{-\gamma}$ approximately holds (γ is the adiabatic index), and in the linear acoustic approximation

$$\frac{p'}{p_0}=\gamma\frac{\rho'}{\rho_0} \tag{3.21}$$

which is identical to (3.10) since $c_0^2=\gamma p_0/\rho_0$.

Combining (3.19)–(3.21) and (3.10), we arrive at

$$\mu=\mu_0\left[1+n(\gamma-1)\frac{p'}{\rho_0c_0^2}\right]. \tag{3.22}$$

With the help of (3.10) we can rearrange $\rho=\rho_0\left(1+\rho'/\rho_0\right)$ to the form

$$\rho=\rho_0\left(1+\frac{p'}{\rho_0c_0^2}\right). \tag{3.23}$$

Combining (3.22) and (3.23), we obtain in the linear acoustic approximation

$$v=v_0\left\{1+[n(\gamma-1)-1]\frac{p'}{\rho_0c_0^2}\right\}. \tag{3.24}$$

Accounting for the fact that in the boundary layer $\partial p'/\partial y=0$ and, as a result, from (3.22) $\partial\mu/\partial y=0$, we obtain from (3.1*b*) the momentum equation in its final form

$$\frac{\partial u}{\partial t}+u\frac{\partial u}{\partial x}+v\frac{\partial u}{\partial y}=\frac{\partial U}{\partial t}+U\frac{\partial U}{\partial x}+v_0\left\{1+[n(\gamma-1)-1]\frac{p'}{\rho_0c_0^2}\right\}\frac{\partial^2u}{\partial y^2}. \tag{3.25}$$

In this equation p' and U are given by (3.5) and (3.7).

Summarizing this section, we note that the equations describing the acoustic streaming arising in the boundary layer near a droplet are (3.17) and (3.25).

4. Acoustic streaming

A solution of the boundary layer equations (3.17) and (3.25) may be obtained by applying the method of successive approximations outlined in Schlichting (1932, 1979). Bearing in mind (3.8) and (3.9), we obtain the estimates

$$\frac{\partial u}{\partial t} \sim B\omega, \qquad u\frac{\partial u}{\partial x} \sim v\frac{\partial u}{\partial y} \sim \frac{B^2}{a}, \tag{4.1a,b}$$

$$\frac{\partial U}{\partial t} \sim B\omega, \quad U\frac{\partial U}{\partial x} \sim \frac{B^2}{a}. \tag{4.1c,d}$$

Also according to (3.5), (2.2) and (2.5*b*)

$$\frac{p'}{\rho_0 c_0^2} \sim \frac{A_{0e}}{\rho_0 c_0^2} = \frac{B}{c_0} = \frac{B}{\omega a}\Omega. \tag{4.2}$$

In the case at hand, $\Omega = O(1)$ which yields

$$\frac{p'}{\rho_0 c_0^2} \sim \frac{B}{\omega a}. \tag{4.3}$$

Also

$$\frac{\partial^2 u}{\partial y^2} \sim B\frac{\omega}{2\nu_0}. \tag{4.4}$$

Combining (4.3) and (4.4), we obtain the estimates

$$\nu_0\frac{\partial^2 u}{\partial y^2} \sim B\omega, \qquad \nu_0\,[n(\gamma-1)-1]\,\frac{p'}{\rho_0 c_0^2}\frac{\partial^2 u}{\partial y^2} \sim \frac{B^2}{a}. \tag{4.5}$$

Terms of the order B^2/a in (4.1) and (4.5) (and thus in (3.25)) are much smaller than those of the order $B\omega$ according to (2.3), which allows us to apply the method of successive approximations to solve (3.25). Thus we employ the asymptotic expansions

$$u = u_0(x,y,t) + u_1(x,y,t), \quad v = v_0(x,y,t) + v_1(x,y,t) \tag{4.6a,b}$$

with

$$\left.\begin{aligned} &u_0 \sim B, \quad u_1 \sim \varepsilon B, \quad \varepsilon = \frac{B}{\omega a} \ll 1, \\ &v_0 \sim \frac{B}{a}\left(\frac{2\nu_0}{\omega}\right)^{1/2}, \quad v_1 \sim \varepsilon\frac{B}{a}\left(\frac{2\nu_0}{\omega}\right)^{1/2}, \end{aligned}\right\} \tag{4.7}$$

where the last two estimates of (4.7) are related to (3.9).

Substituting (4.6) in (3.25), we obtain in the leading order ($B\omega$) according to (4.1), (4.5) and (4.7) the equation

$$\frac{\partial u_0}{\partial t} = \nu_0\frac{\partial^2 u_0}{\partial y^2} + \frac{\partial U}{\partial t}, \tag{4.8a}$$

$$y = 0, \quad u_0 = 0, \tag{4.8b}$$

$$y = \infty, \quad u_0 = U = A(x)\cos\omega t + A_1(x)\sin\omega t. \tag{4.8c}$$

The boundary conditions (4.8*b*, *c*) show that the solution of (4.8*a*) is subject to the no-slip and matching conditions. The boundary condition (4.8*b*) neglects the internal circulation of liquid inside the droplet in the leading order. This assumption is supported by the estimates in Appendix B.

According to (3.7) and (2.2)

$$A(x) = B\frac{c_0}{\omega}\frac{\partial p_{si}}{\partial x}, \tag{4.9a}$$

$$A_1(x) = B\frac{c_0}{\omega}\left(\sin\frac{\omega z_1}{c_0}\frac{\omega}{c_0}\frac{\partial z}{\partial x} - \frac{\partial p_{sr}}{\partial x}\right). \tag{4.9b}$$

The solution of (4.8) is given by

$$u_0 = A(x)\left[\cos\omega t - \mathrm{e}^{-\eta}\cos(\omega t - \eta)\right] + A_1(x)\left[\sin\omega t - \mathrm{e}^{-\eta}\sin(\omega t - \eta)\right], \tag{4.10a}$$

$$\eta = y\left(\frac{\omega}{2v_0}\right)^{1/2}. \tag{4.10b}$$

Substituting expansions (4.6) into the continuity equation (3.17), we arrive in the leading order at

$$\frac{\partial u_0 r}{\partial x} + \frac{\partial v_0 r}{\partial y} = -r\frac{\omega}{c_0}B\left[-\left(\cos\frac{\omega z_1}{c_0} + p_{sr}\right)\sin\omega t + p_{si}\cos\omega t\right]. \tag{4.11}$$

Substituting (4.10a) into (4.11) and integrating, we obtain for v_0 the equation

$$\begin{aligned} v_0 = -\left(\frac{\omega}{2v_0}\right)^{-1/2}\Bigg\{&\left(\frac{\mathrm{d}A}{\mathrm{d}x} + \frac{\mathrm{d}r/\mathrm{d}x}{r}A\right)\\ &\times\left[\eta\cos\omega t - \tfrac{1}{2}\mathrm{e}^{-\eta}(-\cos\eta + \sin\eta)\cos\omega t - \tfrac{1}{2}\mathrm{e}^{-\eta}\right.\\ &\left.\times(-\sin\eta - \cos\eta)\sin\omega t - \tfrac{1}{2}\cos\omega t - \tfrac{1}{2}\sin\omega t\right]\\ &+\left(\frac{\mathrm{d}A_1}{\mathrm{d}x} + \frac{\mathrm{d}r/\mathrm{d}x}{r}A_1\right)\left[\eta\sin\omega t - \tfrac{1}{2}\mathrm{e}^{-\eta}(-\cos\eta + \sin\eta)\sin\omega t\right.\\ &\left.+\tfrac{1}{2}\mathrm{e}^{-\eta}(-\sin\eta - \cos\eta)\cos\omega t - \tfrac{1}{2}\sin\omega t + \tfrac{1}{2}\cos\omega t\right]\\ &+\eta\frac{\omega}{c_0}B\left[-\left(\cos\frac{\omega z_1}{c_0} + p_{sr}\right)\sin\omega t + p_{si}\cos\omega t\right]\Bigg\}. \end{aligned} \tag{4.12}$$

Separating the terms of the order $B\omega\varepsilon$ in (3.25), we arrive at the equation

$$\frac{\partial u_1}{\partial t} - v_0\frac{\partial^2 u_1}{\partial y^2} = U\frac{\partial U}{\partial x} - u_0\frac{\partial u_0}{\partial x} - v_0\frac{\partial u_0}{\partial y} + v_0\left[n(\gamma - 1) - 1\right]\frac{p'}{\rho_0 c_0^2}\frac{\partial^2 u_0}{\partial y^2} \tag{4.13}$$

subject to the boundary conditions

$$y = 0, \quad u_1 = 0; \qquad y = \infty, \quad \frac{\partial u_1}{\partial y} = 0\,. \tag{4.14}$$

The boundary condition for $y = 0$ in (4.14) neglects the internal circulation of liquid inside the droplet of $O(\varepsilon B)$, which is supported by the calculations and estimates in Appendix B.

Our goal is to find a steady average component of the secondary flow u_1, namely $\langle u_1\rangle$, where the averaging is carried out over many cycles of the sound wave, which means that

$$\langle\cos^2\omega t\rangle = \langle\sin^2\omega t\rangle = \tfrac{1}{2}, \quad \langle\sin\omega t\cos\omega t\rangle = 0. \tag{4.15a,b}$$

Since $\langle\partial u_1/\partial t\rangle = 0$, equation (4.13), being averaged, reduces to

$$-\frac{\omega}{2}\frac{\partial^2\langle u_1\rangle}{\partial\eta^2} = \left\langle U\frac{\partial U}{\partial x} - u_0\frac{\partial u_0}{\partial x} - v_0\frac{\partial u_0}{\partial y} + v_0\left[n(\gamma - 1) - 1\right]\frac{p'}{\rho_0 c_0^2}\frac{\partial^2 u_0}{\partial y^2}\right\rangle. \tag{4.16}$$

This equation is integrated accounting for (4.10*a*), (4.12), boundary condition (4.14) for $y = \infty$, as well as the expression for U in (4.8*c*), and (4.15), which yields

$$\begin{aligned}
\langle u_1 \rangle = {} & C + \frac{1}{\omega}\left(A\frac{\mathrm{d}A}{\mathrm{d}x} + A_1\frac{\mathrm{d}A_1}{\mathrm{d}x}\right) \\
& \times \left[\mathrm{e}^{-\eta}\left(2\sin\eta + \tfrac{1}{2}\cos\eta\right) + \frac{\eta\mathrm{e}^{-\eta}}{2}\left(-\cos\eta + \sin\eta\right) + \frac{\mathrm{e}^{-2\eta}}{4}\right] \\
& + \frac{1}{\omega}\frac{\mathrm{d}r/\mathrm{d}x}{r}\left(A^2 + A_1^2\right)\left[\mathrm{e}^{-\eta}\left(\sin\eta + \tfrac{1}{2}\cos\eta\right) + \frac{\eta\mathrm{e}^{-\eta}}{2}\left(-\cos\eta + \sin\eta\right)\right] \\
& - \frac{1}{\omega}\left(A\frac{\mathrm{d}A_1}{\mathrm{d}x} - A_1\frac{\mathrm{d}A}{\mathrm{d}x}\right)\left[\frac{\eta\mathrm{e}^{-\eta}}{2}\left(\sin\eta + \cos\eta\right) + \tfrac{1}{2}\mathrm{e}^{-\eta}\cos\eta - \mathrm{e}^{-\eta}\sin\eta - \frac{\mathrm{e}^{-2\eta}}{4}\right] \\
& + \frac{B}{2c_0}\Bigg\{A\Bigg[\left(\eta\mathrm{e}^{-\eta}\cos\eta + \mathrm{e}^{-\eta}\cos\eta - \mathrm{e}^{-\eta}\sin\eta\right)\left(\cos\frac{\omega z_1}{c_0} + p_{sr}\right) \\
& + \left(\eta\mathrm{e}^{-\eta}\sin\eta + \mathrm{e}^{-\eta}\sin\eta + \mathrm{e}^{-\eta}\cos\eta\right)\left(\cos\frac{\omega z_1}{c_0} + p_{sr}\right)\Bigg] \\
& + A_1\Bigg[-\left(\eta\mathrm{e}^{-\eta}\sin\eta + \mathrm{e}^{-\eta}\sin\eta + \mathrm{e}^{-\eta}\cos\eta\right)\left(\cos\frac{\omega z_1}{c_0} + p_{sr}\right) \\
& + \left(\eta\mathrm{e}^{-\eta}\cos\eta + \mathrm{e}^{-\eta}\cos\eta - \mathrm{e}^{-\eta}\sin\eta\right)\left(\cos\frac{\omega z_1}{c_0} + p_{sr}\right)\Bigg] \\
& + Ap_{si}\left(\eta\mathrm{e}^{-\eta}\sin\eta + \mathrm{e}^{-\eta}\sin\eta - \eta\mathrm{e}^{-\eta}\cos\eta + \mathrm{e}^{-\eta}\sin\eta\right) \\
& + A_1p_{si}\left(\eta\mathrm{e}^{-\eta}\cos\eta + \mathrm{e}^{-\eta}\cos\eta + \eta\mathrm{e}^{-\eta}\sin\eta + \mathrm{e}^{-\eta}\cos\eta\right)\Bigg\} \\
& + \left[n\left(\gamma - 1\right) - 1\right]\frac{B}{2c_0}\Bigg[Ap_{si}\mathrm{e}^{-\eta}\sin\eta + A\mathrm{e}^{-\eta}\cos\eta\left(\cos\frac{\omega z_1}{c_0} + p_{sr}\right) \\
& - A_1\mathrm{e}^{-\eta}\sin\eta\left(\cos\frac{\omega z_1}{c_0} + p_{sr}\right) + A_1p_{si}\mathrm{e}^{-\eta}\cos\eta\Bigg]. \qquad (4.17)
\end{aligned}$$

The constant of integration C in (4.17) is defined by the no-slip condition for $\langle u_1 \rangle$ following from the boundary condition (4.14) for $y = 0$, namely $\langle u_1 \rangle = 0$ at $\eta = 0$ (cf. (B 7) of Appendix B), which yields

$$\begin{aligned}
C = {} & -\frac{1}{\omega}\left(A\frac{\mathrm{d}A}{\mathrm{d}x} + A_1\frac{\mathrm{d}A_1}{\mathrm{d}x}\right)\frac{3}{4} - \frac{1}{\omega}\frac{\mathrm{d}r/\mathrm{d}x}{r}\left(A^2 + A_1^2\right)\frac{1}{2} + \frac{1}{\omega}\left(A\frac{\mathrm{d}A_1}{\mathrm{d}x} - A_1\frac{\mathrm{d}A}{\mathrm{d}x}\right)\frac{1}{4} \\
& - \frac{B}{c_0}\left\{1 + \frac{\left[n\left(\gamma - 1\right) - 1\right]}{2}\right\}\left[A\left(\cos\frac{\omega z_1}{c_0} + p_{sr}\right) + A_1p_{si}\right]. \qquad (4.18)
\end{aligned}$$

It is seen from (4.17) that outside the acoustic boundary layer, as $\eta \to \infty$, an average steady secondary flow exists, since $\langle u_1 \rangle$ tends to the limiting velocity C

$$\langle u_1 \rangle \to C \quad \text{as} \quad \eta \to \infty. \qquad (4.19)$$

This flow is called acoustic streaming. Denoting $\langle u_1 \rangle|_{\eta\to\infty} = \langle u_{1\infty} \rangle$, we obtain from

(4.17) and (4.18) the expression for the acoustic streaming velocity

$$\langle u_{1\infty}\rangle = -\frac{1}{\omega}\left(A\frac{\mathrm{d}A}{\mathrm{d}x}+A_1\frac{\mathrm{d}A_1}{\mathrm{d}x}\right)\frac{3}{4}-\frac{1}{\omega}\frac{\mathrm{d}r/\mathrm{d}x}{r}\left(A^2+A_1^2\right)\frac{1}{2}+\frac{1}{\omega}\left(A\frac{\mathrm{d}A_1}{\mathrm{d}x}-A_1\frac{\mathrm{d}A}{\mathrm{d}x}\right)\frac{1}{4}$$
$$-\frac{B}{c_0}\left\{1+\frac{[n(\gamma-1)-1]}{2}\right\}\left[A\left(\cos\frac{\omega z_1}{c_0}+p_{sr}\right)+A_1 p_{si}\right]. \tag{4.20}$$

The velocity field of the acoustic streaming arising at the outer boundary of the acoustic boundary layer is sketched in figures 2(*a*) and 2(*b*) (the corresponding numerical results are depicted in figures 14(*a*)–14(*e*) below).

The inner acoustic streaming also generates a system of large-scale toroidal vortices about the droplet, the so-called outer acoustic streaming. In simple levitators without any additional blowing, these vortices were found experimentally in Trinh & Robey (1994). They were also calculated in Riley (1966) and Lee & Wang (1990). The vortices are shown schematically in figure 2(*c*), and represent almost closed recirculation zones. There are several possible causes for such vortices. Among them are the interaction of the flow with the confinement walls, the displacement of the droplet from the pressure nodal point, and the interaction with another superimposed flow. In the first case the characteristic scale L_* of the vortices should be of the order of the cross-sectional diameter of the confinement (and thus much larger than the initial volume-equivalent droplet radius a_0). In the other cases L_* is of the order of several droplet radii.

In the case of a superimposed external blowing along the levitator axis (like that of Seaver *et al.* 1989; Seaver & Peele 1990; Trinh & Robey 1994 and Yarin *et al.* 1997), or normal to it as in the present work, the vortices may be ventilated by the external stream. Experimental evidence of Trinh & Robey (1994) and of the present work supports the idea of such ventilation. These vortices and their ventilation due to external blowing have an important effect on the droplet evaporation rate (see the discussion in § 8 and § 9 below).

5. Incompressible limit of the inner acoustic streaming in the case of a small spherical particle

The displacement of a very small light particle from the pressure node becomes negligibly small compared to the sound wavelength. Thus we consider a particle positioned at a pressure node. Therefore, its displacement from the pressure antinode (see figure 1) is

$$L = \frac{\pi c_0}{2\omega}. \tag{5.1}$$

Therefore we find

$$\frac{\omega z_1}{c_0} = \frac{\omega z}{c_0}+\frac{\pi}{2}. \tag{5.2}$$

Since $z \sim a$, the term $\omega z/c_0 \sim \omega a/c_0 = \Omega \ll 1$ in the present case (the long-wave, incompressible limit which we consider in this section), and thus

$$\frac{\omega z_1}{c_0} = \frac{\pi}{2}. \tag{5.3}$$

Also the non-dimensional Helmholtz equation (3.4) reads

$$\bar{\Delta} p_s + \Omega^2 p_s = 0, \tag{5.4}$$

where $\bar{\Delta}$ denotes the non-dimensional Laplacian with the coordinates scaled by a.

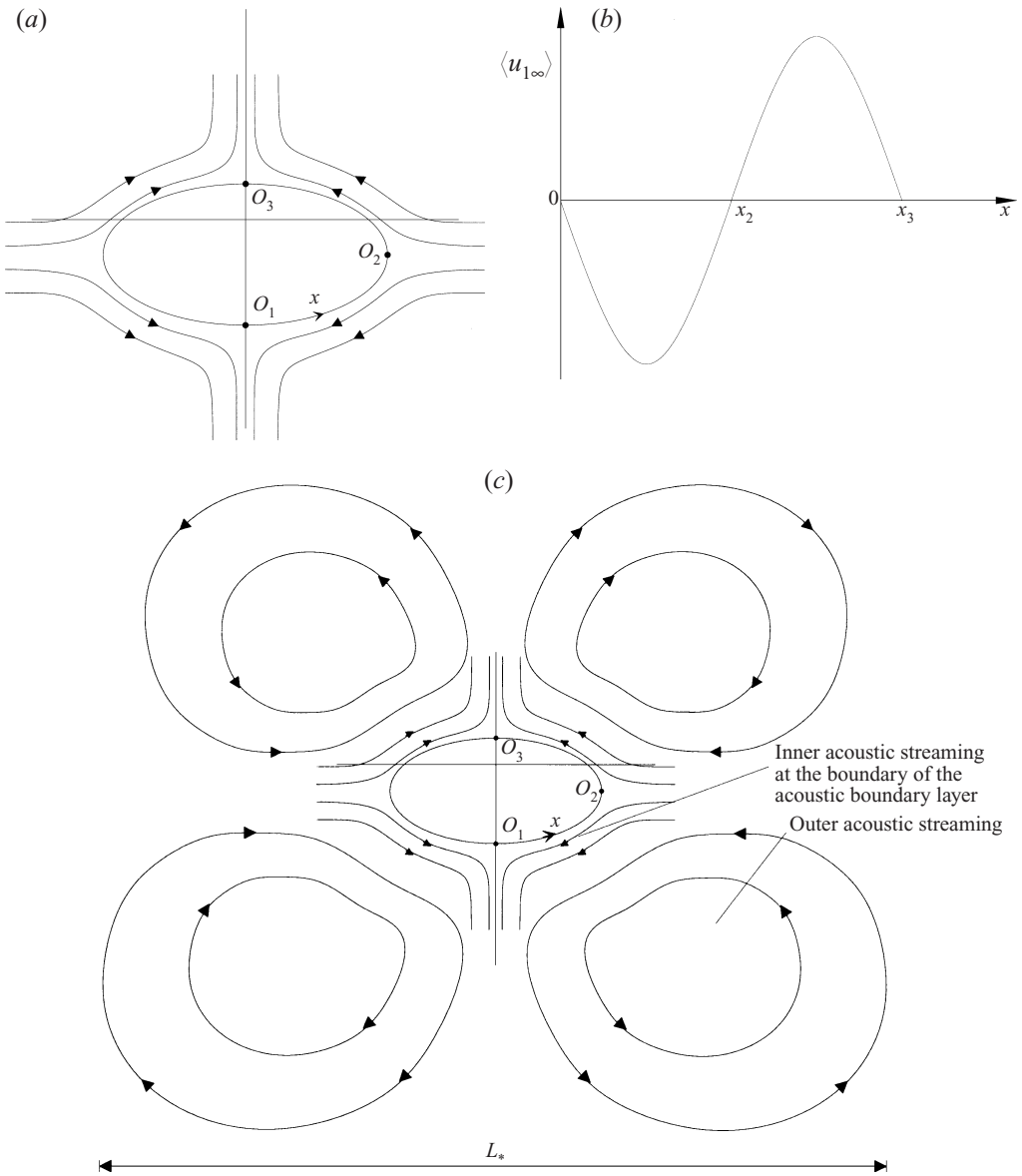

FIGURE 2. Sketches of the acoustic streaming field near the levitated droplet and the system of the outer toroidal vortices. (*a*) The streamlines of the average secondary flow near the outer boundary of the acoustic boundary layer. (*b*) The distribution of $\langle u_{1\infty} \rangle$ over the droplet surface. x is the arclength of the droplet generatrix from the bottom O_1; x_2 and x_3 correspond to points O_2 and O_3. (*c*) The outer toroidal vortices (the outer acoustic streaming flow) emerging in the space of the levitator.

For $\Omega \ll 1$ the last term in (5.4) is negligibly small, and Laplace equations for the real and imaginary parts of p_s

$$\Delta p_{sr} = 0, \qquad \Delta p_{si} = 0 \tag{5.5}$$

emerge with

$$p_{sr} \to 0, \qquad p_{si} \to 0 \quad \text{as } R \to \infty, \tag{5.6}$$

where R is the radial spherical coordinate ($R = 0$ at the particle centre coincident with the pressure node).

The boundary conditions at the surface of the particle (assumption (ii) in § 2) correspond to $\partial p/\partial R = 0$ at $R = a$. Accounting for (3.2) and (3.3a), we obtain the boundary conditions at the sphere surface

$$\frac{\partial p_{sr}}{\partial R} = -\frac{\partial}{\partial R}\left[\cos\left(\frac{\omega z_1}{c_0}\right)\right], \quad \frac{\partial p_{si}}{\partial R} = 0 \quad \text{at } R = a. \tag{5.7a, b}$$

From the Laplace equation for p_{si} in (5.5), and the conditions for p_{si} in (5.6) and (5.7b) we obtain

$$p_{si} \equiv 0, \tag{5.8}$$

whereas, accounting for the geometric expression

$$\frac{\partial}{\partial R} = -\frac{\partial z}{\partial x}\frac{\partial}{\partial r} + \frac{\partial r}{\partial x}\frac{\partial}{\partial z} \tag{5.9}$$

condition (5.7a) yields

$$\frac{\partial p_{sr}}{\partial R} = -\frac{\partial r}{\partial x}\frac{\omega}{c_0}\sin\frac{\omega z_1}{c_0} = -\frac{\partial r}{\partial x}\frac{\omega}{c_0} \quad \text{at } R = a. \tag{5.10}$$

Note that the last equality in (5.10) follows from (5.3).

The r-coordinate of the sphere surface is evidently given by

$$r = a\sin\frac{x}{a} \tag{5.11}$$

whereby

$$\frac{\partial r}{\partial x} = \cos\theta, \quad \theta = \frac{x}{a} \tag{5.12a, b}$$

in which θ is the angular spherical coordinate reckoned from the levitator axis (see figure 1).

Due to (5.10) and (5.12a) the boundary condition for p_{sr} at the sphere surface reads

$$\frac{\partial p_{sr}}{\partial R} = -\frac{\omega}{c_0}\cos\theta \quad \text{at } R = a. \tag{5.13}$$

The solution of the Laplace equation for p_{sr} in (5.5) satisfying the conditions for p_{sr} in (5.6) and (5.13) is given by

$$p_{sr} = \frac{\omega a^3}{2c_0}\frac{\cos\theta}{R^2} \tag{5.14}$$

which yields

$$p_{sr} = \frac{\omega a}{2c_0}\cos\theta = \frac{\omega a}{2c_0}\cos\frac{x}{a} \quad \text{at } R = a. \tag{5.15}$$

Substituting (5.8), (5.15) and (5.3) into (4.9) and accounting for the fact that

$$z = a\left(1 - \cos\frac{x}{a}\right), \quad \frac{\partial z}{\partial x} = \sin\frac{x}{a}, \tag{5.16}$$

we arrive at

$$A \equiv 0, \quad A_1 = \frac{3}{2}B\sin\frac{x}{a}. \tag{5.17}$$

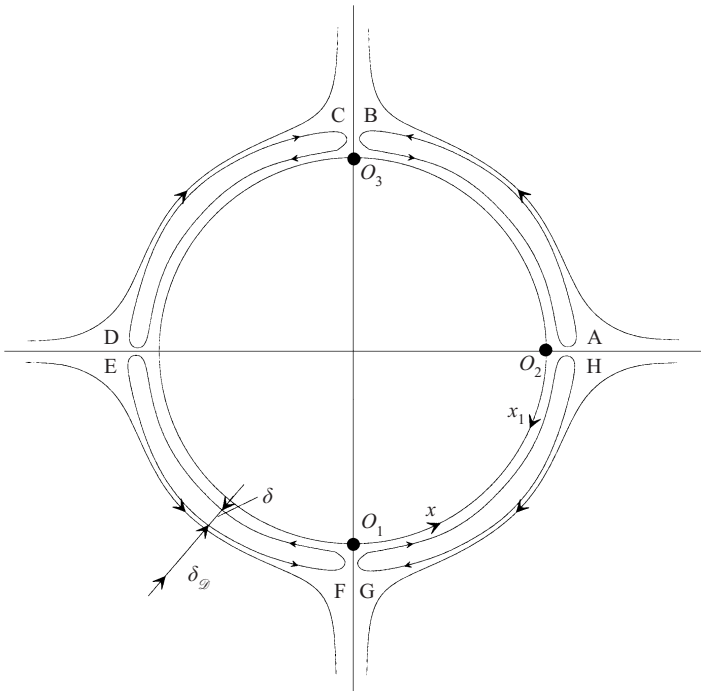

FIGURE 3. Sketch of the acoustic streaming over a small sphere positioned at the pressure node. The thicknesses of the acoustic and diffusion boundary layers, δ and $\delta_{\mathscr{D}}$, are also shown schematically. The four closed loops inside the acoustic boundary layer AB, CD, EF, and GH represent the whole structure of the steady flow emerging there.

Substituting (5.17), (5.8) and (5.15) into (4.20), we obtain

$$\langle u_{1\infty} \rangle = -\frac{45}{32} \frac{B^2}{\omega a} \sin \frac{2x}{a} \tag{5.18}$$

which yields the well-known pattern of the acoustic streaming near a sphere reproduced in figure 3. The corresponding experimental verifications can be found in Schlichting (1979) and Trinh & Robey (1994) (in the latter work some additional references are given).

Note that expression (5.18) was obtained in Burdukov & Nakoryakov (1965*b*): their (2.8) with $1.406 \approx 45/32$. It also follows from equation (38) of Lee & Wang (1989) and equation (15) of Lee & Wang (1990). According to (5.18) the characteristic scale of the acoustic streaming velocity B_s is given by

$$B_s = \frac{B^2}{\omega a}. \tag{5.19}$$

Since according to the estimates of § 2 $B/(\omega a) \sim 10^{-2}$, equation (5.19) shows that $B_s \sim 10^{-2} B$. According to the estimate of § 2, $B = 352\,\mathrm{cm\,s^{-1}}$. Therefore from (5.19) we obtain $B_s \approx 3.52\,\mathrm{cm\,s^{-1}}$. The streaming Reynolds number Re_s is defined following Stuart (1966) as

$$Re_s = \frac{B_s a}{\nu_0} = \frac{B^2}{\omega \nu_0}. \tag{5.20}$$

For $a \sim 10^{-1}$ cm and $\nu_0 \sim 0.15\,\mathrm{cm^2\,s^{-1}}$, we obtain $Re_s \approx 2.35$.

6. Mass transfer at the surface of the acoustically levitated droplet

We turn back to the general case of the acoustically levitated droplet acquiring an oblate shape and displaced below the pressure node. For the sake of brevity we consider only mass transfer during evaporation. In the case where the SPL is high enough and thus the inner acoustic streaming dominates free convection, and when radiation is neglected, the calculation for heat transfer may be performed similarly, so we refer only to the final result.

Denote the concentration of evaporating (or sublimating) material of the droplet (or particle) in air by c. In what follows the dimension of the concentration is $\mathrm{g\,cm^{-3}}$. The diffusion equation in the boundary layer near the droplet/particle surface reads

$$\rho\left(\frac{\partial c}{\partial t}+u\frac{\partial c}{\partial x}+v\frac{\partial c}{\partial y}\right)=\frac{\partial}{\partial y}\left(\rho\mathscr{D}\frac{\partial c}{\partial y}\right), \tag{6.1}$$

where $\mathscr{D}$ is the mass diffusion coefficient.

Also

$$\mathscr{D}=\mathscr{D}_0+\mathscr{D}', \tag{6.2}$$

where an unperturbed value of the diffusion coefficient is denoted by subscript zero, whereas $\mathscr{D}'$ is a perturbation due to the sound wave.

In general $\mathscr{D}'=\mathscr{D}'(p',\ \rho',\ T')$, however via (3.10) and (3.20) this reduces to the dependence $\mathscr{D}'=\mathscr{D}'(p')$.

The term

$$\frac{\partial\rho\mathscr{D}'}{\partial y}\frac{\partial c}{\partial y}=\left(\frac{\partial p'}{\partial y}\frac{\mathscr{D}'}{c_0^2}+\rho\frac{\partial\mathscr{D}'}{\partial y}\right)\frac{\partial c}{\partial y} \tag{6.3}$$

arising on the right in (6.1) vanishes since in the boundary layer $\partial p'/\partial y=0$. As usual in the theory of the diffusion boundary layer, we expect its thickness $\delta_{\mathscr{D}}$ to be of the order

$$\delta_{\mathscr{D}}\sim\frac{a}{\left(Ba/\mathscr{D}_0\right)^{1/2}} \tag{6.4}$$

accounting for the fact that $\left(v_0/\mathscr{D}_0\right)^{1/2}=O(1)$, which holds for most practically important liquids and certainly for all liquids studied experimentally in § 9.

Since the thickness of the acoustic boundary layer scales as $\delta\sim(2v_0/\omega)^{1/2}$, we obtain

$$\frac{\delta}{\delta_{\mathscr{D}}}=\left(\frac{2v_0}{\mathscr{D}_0}\right)^{1/2}\left(\frac{B}{\omega a}\right)^{1/2}. \tag{6.5}$$

Given $v_0=0.15\,\mathrm{cm^2\,s^{-1}}$ and $\omega=2\pi\times56000\,\mathrm{Hz}$ we find $\delta=(2v_0/\omega)^{1/2}=0.92\times10^{-3}\,\mathrm{cm}$. Also for the characteristic values of $(2v_0/\mathscr{D}_0)^{1/2}\sim1$ and $B/\omega a\sim10^{-2}$ (for the latter cf. § 2) we find from (6.5) that $\delta_{\mathscr{D}}=10\delta=0.92\times10^{-2}\,\mathrm{cm}$. Therefore for $a\sim10^{-1}\,\mathrm{cm}$ the following inequalities hold:

$$\delta\ll\delta_{\mathscr{D}}\ll a. \tag{6.6}$$

This means that, on the one hand, the outer boundary of the acoustic boundary layer practically coincides with the droplet/particle surface when one considers mass transfer. On the other hand, the outer boundary of the diffusion boundary layer still does not extend to the region where the acoustic streaming field begins to vary significantly relative to the values at the outer boundary of the acoustic boundary layer. Indeed, according to Lee & Wang (1990), such a variation in the outer streaming flow is felt on the scales of the order of several droplet radii. Therefore, as a plausible

approximation we can assume that the velocity components $u = u_0 + u_1$ and $v = v_0 + v_1$ in (6.1) (throughout the diffusion boundary layer) correspond in reality to those at the outer boundary of the inner acoustic boundary layer, which is denoted below by subscript ∞.

We also split the concentration field into a steady (c_s) and an unsteady part (c_u), as $c = c_s + c_u$, where $\partial c_s/\partial t = 0$. Therefore accounting for (6.2), we transform equation (6.1) to the form

$$\frac{\partial c_u}{\partial t} + u_{0\infty}\frac{\partial c_s}{\partial x} + u_{0\infty}\frac{\partial c_u}{\partial x} + u_{1\infty}\frac{\partial c_s}{\partial x} + u_{1\infty}\frac{\partial c_u}{\partial x} + v_{0\infty}\frac{\partial c_s}{\partial y} + v_{0\infty}\frac{\partial c_u}{\partial y} + v_{1\infty}\frac{\partial c_s}{\partial y} + v_{1\infty}\frac{\partial c_u}{\partial y} = \mathscr{D}_0\frac{\partial^2 c_s}{\partial y^2} + \mathscr{D}_0\frac{\partial^2 c_u}{\partial y^2} + \mathscr{D}'\frac{\partial^2 c_s}{\partial y^2} + \mathscr{D}'\frac{\partial^2 c_u}{\partial y^2}. \quad (6.7)$$

According to (4.6), (4.7) and (2.3)

$$\frac{u_{1\infty}}{u_{0\infty}} \sim \frac{B}{\omega a} \ll 1, \qquad \frac{v_{1\infty}}{v_{0\infty}} \sim \frac{B}{\omega a} \ll 1 \quad (6.8)$$

which allows us to neglect in (6.7) the terms $u_{1\infty}\partial c_s/\partial x + u_{1\infty}\partial c_u/\partial x$ and $v_{1\infty}\partial c_s/\partial y + v_{1\infty}\partial c_u/\partial y$ compared to the corresponding terms containing $u_{0\infty}$ and $v_{0\infty}$.

Also at high ultrasonic frequencies (which is our case) we can expect that $c_u \ll c_s$, which we prove *a posteriori* below. As a result of this assumption, we can neglect in (6.7) the terms $u_{0\infty}\partial c_u/\partial x$ and $v_{0\infty}\partial c_u/\partial y$ as compared to the corresponding terms containing c_s.

To show that $c_u \ll c_s$ at high ultrasonic frequencies, we notice the following. Far enough from the droplet we expect the diffusion terms on the right in (6.7) to be weak compared to the remaining convective terms on the left, as previously was assumed by Lighthill (1954) (cf. his equation (5.9)). Thus neglecting the diffusion term, we arrive at the final form of the instantaneous diffusion equation

$$\frac{\partial c_u}{\partial t} + u_{0\infty}\frac{\partial c_s}{\partial x} + v_{0\infty}\frac{\partial c_s}{\partial y} = 0 \quad (6.9)$$

which yields after integration the unsteady part of the concentration as

$$c_u = -\frac{\partial c_s}{\partial x}\int u_{0\infty}\,\mathrm{d}t - \frac{\partial c_s}{\partial y}\int v_{0\infty}\,\mathrm{d}t. \quad (6.10)$$

Since according to (4.10*a*) and (4.12)

$$\int u_{0\infty}\,\mathrm{d}t \sim \frac{1}{\omega}, \quad \int v_{0\infty}\,\mathrm{d}t \sim \frac{1}{\omega}, \quad (6.11)$$

we see that c_u indeed tends to zero as $\omega \to \infty$, as expected.

Using (6.9), we obtain

$$\left\langle u_{0\infty}\frac{\partial c_u}{\partial x} + v_{0\infty}\frac{\partial c_u}{\partial y}\right\rangle = -\frac{\partial^2 c_s}{\partial x^2}\left\langle u_{0\infty}\int u_{0\infty}\,\mathrm{d}t\right\rangle - \frac{\partial c_s}{\partial x}\left\langle u_{0\infty}\int \frac{\partial u_{0\infty}}{\partial x}\,\mathrm{d}t\right\rangle - \frac{\partial^2 c_s}{\partial x\partial y}\left\langle u_{0\infty}\int v_{0\infty}\,\mathrm{d}t\right\rangle - \frac{\partial c_s}{\partial y}\left\langle u_{0\infty}\int \frac{\partial v_{0\infty}}{\partial x}\,\mathrm{d}t\right\rangle - \frac{\partial^2 c_s}{\partial x\partial y}\left\langle v_{0\infty}\int u_{0\infty}\,\mathrm{d}t\right\rangle - \frac{\partial^2 c_s}{\partial y^2}\left\langle v_{0\infty}\int v_{0\infty}\,\mathrm{d}t\right\rangle - \frac{\partial c_s}{\partial y}\left\langle v_{0\infty}\int \frac{\partial v_{0\infty}}{\partial y}\,\mathrm{d}t\right\rangle. \quad (6.12)$$

The calculation of the correlations on the right in (6.12) is given in Appendix A.

Accounting for (A 2) and (A 3), we obtain

$$\left\langle u_{0\infty}\frac{\partial c_u}{\partial x}+v_{0\infty}\frac{\partial c_u}{\partial y}\right\rangle=-\frac{1}{2\omega}\left(-A\frac{\mathrm{d}A_1}{\mathrm{d}x}+A_1\frac{\mathrm{d}A}{\mathrm{d}x}\right)\frac{\partial c_s}{\partial x}+O\left(B\frac{B}{\omega a}\frac{\delta}{a}\right)\frac{\partial c_s}{\partial y}. \tag{6.13}$$

Averaging equation (6.7) in time, we obtain

$$\langle u_{1\infty}\rangle\frac{\partial c_s}{\partial x}+\langle v_{1\infty}\rangle\frac{\partial c_s}{\partial y}=\mathscr{D}_0\frac{\partial^2 c_s}{\partial y^2}-\left\langle u_{0\infty}\frac{\partial c_u}{\partial x}+v_{0\infty}\frac{\partial c_u}{\partial y}\right\rangle+\left\langle\mathscr{D}'\frac{\partial^2 c_u}{\partial y^2}\right\rangle, \tag{6.14}$$

whereas the continuity equation (3.17), accounting for (4.6), yields for the components of the average acoustic streaming

$$\frac{\partial\left(\langle u_{1\infty}\rangle r\right)}{\partial x}+\frac{\partial\left(\langle v_{1\infty}\rangle r\right)}{\partial y}=0. \tag{6.15}$$

Integrating (6.15), we arrive at

$$\langle v_{1\infty}\rangle=-\frac{1}{r}\frac{\partial\left(\langle u_{1\infty}\rangle r\right)}{\partial x}y. \tag{6.16}$$

In the diffusion boundary layer $y\sim\delta_{\mathscr{D}}$, $x\sim a$ and therefore from (6.16)

$$\langle v_{1\infty}\rangle\sim\frac{\delta_{\mathscr{D}}}{a}\langle u_{1\infty}\rangle \tag{6.17}$$

and also

$$\frac{\partial c_s}{\partial x}\sim\frac{\delta_{\mathscr{D}}}{a}\frac{\partial c_s}{\partial y}. \tag{6.18}$$

Using (6.16) and (6.17), we estimate

$$\langle u_{1\infty}\rangle\frac{\partial c_s}{\partial x}+\langle v_{1\infty}\rangle\frac{\partial c_s}{\partial y}\sim\frac{\delta_{\mathscr{D}}}{a}\langle u_{1\infty}\rangle\frac{\partial c_s}{\partial y}. \tag{6.19}$$

Expressions (6.13) and (6.19) allow us to estimate the ratio

$$\frac{\langle u_{0\infty}\partial c_u/\partial x+v_{0\infty}\partial c_u/\partial y\rangle}{\langle u_{1\infty}\rangle\partial c_s/\partial x+\langle v_{1\infty}\rangle\partial c_s/\partial y}\sim\frac{-(2\omega)^{-1}\left(-A\mathrm{d}A_1/\mathrm{d}x+A_1\mathrm{d}A/\mathrm{d}x\right)\partial c_s/\partial x}{\langle u_{1\infty}\rangle\left(\delta_{\mathscr{D}}/a\right)\partial c_s/\partial y}+O\left(\frac{B^2}{\omega a}\frac{\delta}{\delta_{\mathscr{D}}}\frac{1}{\langle u_{1\infty}\rangle}\right). \tag{6.20}$$

Recalling (6.18) as well as the fact that $\langle u_{1\infty}\rangle\sim B^2/(\omega a)$, (6.20) may be written as

$$\frac{\langle u_{0\infty}\partial c_u/\partial x+v_{0\infty}\partial c_u/\partial y\rangle}{\langle u_{1\infty}\rangle\partial c_s/\partial x+\langle v_{1\infty}\rangle\partial c_s/\partial y}\sim\frac{-(2\omega)^{-1}\left(-A\mathrm{d}A_1/\mathrm{d}x+A_1\mathrm{d}A/\mathrm{d}x\right)}{\langle u_{1\infty}\rangle}+O\left(\frac{\delta}{\delta_{\mathscr{D}}}\right). \tag{6.21}$$

According to (4.20) the first term on the right in (6.21) is of the order of one, whereas according to (6.6) the second term is negligibly small. This leads to the conclusion that only the first term on the right in (6.13) cannot be neglected after substitution in (6.14) compared to the left-hand side of (6.14). As a result, (6.14) takes the form

$$\langle u_{1\infty}\rangle\frac{\partial c_s}{\partial x}+\langle v_{1\infty}\rangle\frac{\partial c_s}{\partial y}=\mathscr{D}_0\frac{\partial^2 c_s}{\partial y^2}+\frac{1}{2\omega}\left(-A\frac{\mathrm{d}A_1}{\mathrm{d}x}+A_1\frac{\mathrm{d}A}{\mathrm{d}x}\right)\frac{\partial c_s}{\partial x}+\left\langle\mathscr{D}'\frac{\partial^2 c_u}{\partial y^2}\right\rangle. \tag{6.22}$$

To deal with the last term of equation (6.22), we introduce the Schmidt number Sc, as $\mathscr{D} = \nu/Sc$. Then using (3.24), we obtain

$$\mathscr{D} = \mathscr{D}_0 \left\{ 1 + [n(\gamma - 1) - 1] \frac{p'}{\rho_0 c_0^2} \right\}, \quad \mathscr{D}_0 = \nu_0/Sc. \tag{6.23a,b}$$

A plausible assumption for gases is $n \approx 1$ and $\gamma \approx 1.4$. Therefore $n(\gamma - 1) - 1 \approx -0.6$. Since in the parameter range of the present work $p'/\left(\rho_0 c_0^2\right) \sim A_{0e}/\left(\rho_0 c_0^2\right) \sim 10^{-2}$, the sound term on the right in (6.23a) is negligibly small as compared to the first one, and thus $\mathscr{D}'$ is negligibly small. Note also that the term $[n(\gamma - 1) - 1]/2$ is of the order of 0.1 and may be neglected as compared to 1 to simplify the expression for $\langle u_{1\infty} \rangle$ in (4.20).

Equation (6.22) reduces now to the form

$$\langle \tilde{u}_{1\infty} \rangle \frac{\partial c_s}{\partial x} + \langle v_{1\infty} \rangle \frac{\partial c_s}{\partial y} = \mathscr{D}_0 \frac{\partial^2 c_s}{\partial y^2} \tag{6.24a}$$

$$\langle \tilde{u}_{1\infty} \rangle = \langle u_{1\infty} \rangle - \frac{1}{2\omega} \left(-A \frac{\mathrm{d}A_1}{\mathrm{d}x} + A_1 \frac{\mathrm{d}A}{\mathrm{d}x} \right). \tag{6.24b}$$

Substituting (6.16) into (6.24a), we obtain

$$\frac{\partial^2 c_s}{\partial y^2} + P(x) y \frac{\partial c_s}{\partial y} = Q(x) \frac{\partial c_s}{\partial x}, \tag{6.25}$$

where

$$P(x) = \frac{1}{\mathscr{D}_0 r} \frac{\partial \langle u_{1\infty} \rangle r}{\partial x}, \qquad Q(x) = \frac{\langle \tilde{u}_{1\infty} \rangle}{\mathscr{D}_0} \tag{6.26}$$

are known functions.

The concentration c_s is subject to the boundary conditions

$$y = 0, \qquad c_s = c_{sb}, \tag{6.27a}$$

$$y = \infty, \qquad c_s = c_{s\infty}, \tag{6.27b}$$

which means that at the surface the concentration is equal to a known value c_{sb}, corresponding to the saturation conditions, whereas far from the droplet it approaches a value $c_{s\infty}$ which is discussed in detail in § 8.

The solution of (6.25) with the boundary conditions (6.27) is given by

$$c_s = c_{s\infty} + (c_{sb} - c_{s\infty}) \left[1 - \mathrm{erf} \left(\frac{Z}{2} \right) \right] \tag{6.28}$$

with

$$Z = y \left[\mathrm{e}^{-W(x)} \int_{x_2}^{x} \frac{\mathrm{e}^{W(\xi)}}{Q(\xi)} \mathrm{d}\xi \right]^{-1/2}, \quad W(x) = 2 \int_{x_2}^{x} \frac{P(\xi)}{Q(\xi)} \mathrm{d}\xi, \tag{6.29a,b}$$

where x_2 is the arclength to the stagnation point O_2 of the inner acoustic streaming flow (figure 2a).

The time-averaged mass transfer coefficient $\langle h \rangle$ is given by

$$\langle h \rangle (c_{sb} - c_{s\infty}) = -\mathscr{D}_0 \frac{\partial c_s}{\partial y}\bigg|_{y=0} \tag{6.30}$$

and thus, via (6.26) and (6.28)–(6.30), we obtain a distribution of the time-averaged Sherwood number $\langle Sh\rangle$ over the droplet surface

$$\langle Sh\rangle = \frac{\langle h\rangle 2a}{\mathscr{D}_0} = \frac{2a}{(\pi\mathscr{D}_0)^{1/2}}\left[\int_{x_2}^{x}\frac{\mathrm{e}^{W(\xi)-W(x)}}{\langle\tilde{u}_{1\infty}(\xi)\rangle}\mathrm{d}\xi\right]^{-1/2}, \tag{6.31}$$

where

$$W(x) = 2\int_{x_2}^{x}\frac{1}{r\langle\tilde{u}_{1\infty}\rangle}\frac{\partial\langle u_{1\infty}\rangle r}{\partial\xi}\mathrm{d}\xi \tag{6.32}$$

and $\langle u_{1\infty}\rangle$ and $\langle\tilde{u}_{1\infty}\rangle$ are given by (4.20) and (6.24*b*), respectively. In (6.31), a is a current volume-equivalent radius of the droplet.

Averaging of $\langle Sh\rangle$ over the droplet surface yields

$$\overline{\langle Sh\rangle} = \int_0^l \langle Sh\rangle r\mathrm{d}x \Big/ \int_0^l r\mathrm{d}x, \tag{6.33}$$

where l is half of the perimeter of the droplet cross-section.

Note that the results (6.31) and (6.33) of this section cannot be extrapolated to the case of vanishing acoustic field ($\omega \to 0$), since they were obtained for $Re = \omega a^2/\nu_0 \gg 1$ and $S^{-1} = B/(\omega a) \ll 1$.

It is emphasized that, regarding the heat transfer problem, one may simply change $\mathscr{D}_0$ on the left in (6.31) for the thermal conductivity of air k_a and $\mathscr{D}_0$ on the right for the thermal diffusivity of air κ_0, and thus obtain from (6.31) and (6.33) the formulae for the Nusselt numbers $\langle Nu\rangle$ and $\overline{\langle Nu\rangle}$. This, however, requires an assumption that the SPL is high enough and the temperature differences are small (and radiation can be neglected), and thus the acoustic streaming flow dominates free convection.

We illustrate the results (6.31) and (6.33), which are the central ones in the present work, in § 9, also comparing them with experimental data. However, we first consider their limiting forms. Numerical examples show that, in many cases, the inequality

$$\left|-A\frac{\mathrm{d}A_1}{\mathrm{d}x} + A_1\frac{\mathrm{d}A}{\mathrm{d}x}\right| \ll \left|A\frac{\mathrm{d}A}{\mathrm{d}x} + A_1\frac{\mathrm{d}A_1}{\mathrm{d}x}\right| \tag{6.34}$$

holds and, as a result, the last term on the right-hand side in (6.24*b*) is negligibly small, and $\langle\tilde{u}_{1\infty}\rangle = \langle u_{1\infty}\rangle$. Thus it follows from (6.32) that

$$\mathrm{e}^{W(\xi)-W(x)} = \left[\frac{\langle u_{1\infty}(\xi)\rangle r(\xi)}{\langle u_{1\infty}(x)\rangle r(x)}\right]^2, \tag{6.35}$$

and consequently (6.31) reduces to

$$\langle Sh\rangle = \frac{2a}{\sqrt{\pi\mathscr{D}_0}}\frac{|\langle u_{1\infty}(x)\rangle|r(x)}{\sqrt{X}}, \tag{6.36a}$$

$$X = \int_{x_2}^{x}\langle u_{1\infty}\rangle r^2\mathrm{d}x \tag{6.36b}$$

which are the limiting forms of (6.31) and (6.32).

7. Incompressible limit of the Sherwood/Nusselt number in the case of a small spherical particle

In the case at hand $A \equiv 0$ and $A_1 = \frac{3}{2}B \sin x/a$, as shown in (5.17). Also, according to (5.18) and (5.11)

$$\langle u_{1\infty} \rangle = -\frac{45}{32}\frac{B^2}{\omega a}\sin\frac{2x}{a}, \quad r = a\sin\frac{x}{a}, \quad x_2 = \frac{\pi}{2}a \tag{7.1a–c}$$

(relation (7.1*c*) defines the arclength between the stagnation points O_1 and O_2).

In the present case (6.34) definitely holds and formulae (6.36) are exact.

Using (7.1) and considering, for example, the part of the droplet below the stagnation point, we obtain from (6.36*b*)

$$X = \frac{45}{64}\frac{B^2a^2}{\omega}\left(1 - \sin^4\frac{x}{a}\right) \tag{7.2}$$

and from (6.36*a*)

$$\begin{aligned}\langle Sh \rangle &= 2\left(\frac{45}{4\pi}\right)^{1/2}\frac{B}{(\omega\mathscr{D}_0)^{1/2}}\frac{\sin^2 x/a}{\left(1+\sin^2 x/a\right)^{1/2}} \\ &= 2\left(\frac{45}{4\pi}\right)^{1/2}\frac{B}{(\omega\mathscr{D}_0)^{1/2}}\frac{\cos^2 x_1/a}{\left(1+\cos^2 x_1/a\right)^{1/2}},\end{aligned} \tag{7.3}$$

where x_1 is the arclength reckoned from the stagnation point O_2 (figure 3). Note that this distribution of $\langle Sh \rangle$ in terms of x_1/a is symmetric about the vertical axis through point O_3 in figure 3 and thus its average over the sphere surface is given by

$$\overline{\langle Sh \rangle} = \frac{2\pi}{4\pi}\int_0^\pi \langle Sh \rangle \cos\frac{x_1}{a}\;\; d\left(\frac{x_1}{a}\right) = \left(\frac{45}{4\pi}\right)^{1/2}\frac{B}{(\omega\mathscr{D}_0)^{1/2}} = 1.89\frac{B}{\sqrt{\omega\mathscr{D}_0}}. \tag{7.4}$$

Formulae (7.3) and (7.4) represent the limit of the results (6.31) and (6.33) in the case of a small spherical particle. It is emphasized that the Sherwood number, according to (7.4), does not depend on the sphere radius a. A formula similar to (7.4) was published and used in Burdukov & Nakoryakov (1965*b*) with an erroneous multiplier (see their equation (3.13) with a factor of 1.3 instead of $(45/4\pi)^{1/2} = 1.89$). As previously mentioned (7.3) and (7.4) cannot be extrapolated into the low-frequency domain. Note also that similar calculations for a cylinder yield $\overline{\langle Sh \rangle} = 1.76B/\sqrt{\omega\mathscr{D}_0}$ (Burdukov & Nakoryakov 1965*a*) and $\overline{\langle Sh \rangle} = (96/\pi^3)^{1/2}B/\sqrt{\omega\mathscr{D}_0} = 1.76B/\sqrt{\omega\mathscr{D}_0}$ (Richardson 1967).

We now apply (7.4) to find the decrease in the radius of a spherical particle evaporating (or sublimating) in the acoustic field. From (7.4) we obtain

$$\overline{\langle h \rangle} = \frac{1}{2}\left(\frac{45}{4\pi}\right)^{1/2}\frac{B}{(\omega\mathscr{D}_0)^{1/2}}\frac{\mathscr{D}_0}{a}. \tag{7.5}$$

Therefore the mass loss per unit time is

$$Q_m = 4\pi a^2\overline{\langle h \rangle}\,(c_{sb} - c_{s\infty}) = 2\pi a\left(\frac{45}{4\pi}\right)^{1/2}B\left(\frac{\mathscr{D}_0}{\omega}\right)^{1/2}(c_{sb} - c_{s\infty}), \tag{7.6}$$

and the mass balance is given by

$$\frac{\mathrm{d}}{\mathrm{d}t}\left(\rho_l\tfrac{4}{3}\pi a^3\right) = -Q_m, \tag{7.7}$$

Liquid	A_*	B_*	C_*	D_*	E_*
Methanol	18.5875	3626.55	−34.29	24.335	0.0856
Ethanol	18.9919	3803.98	−41.68	24.270	0.0878
Propanol-2	17.5439	3166.38	−80.15	25.370	0.0791
n-Heptane	15.8738	2911.32	−56.51	22.332	0.0996
n-Octane	15.9426	3120.29	−63.63	23.493	0.0940
n-Decane	16.0114	3456.80	−78.67	25.731	0.0934

TABLE 1. Liquid parameters used to calculate the saturation pressure of the vapour and surface tension (Reid *et al.* 1987).

a_{0*}	6.107799961
a_{1*}	$4.436518521 \times 10^{-1}$
a_{2*}	$1.428945805 \times 10^{-2}$
a_{3*}	$2.650648731 \times 10^{-4}$
a_{4*}	$3.031240396 \times 10^{-6}$
a_{5*}	$2.034080948 \times 10^{-8}$
a_{6*}	$6.136820929 \times 10^{-11}$

TABLE 2. Parameters used to calculate the saturation pressure of water vapour (Seaver *et al.* 1989).

where ρ_l is the liquid density. Substituting (7.6) in (7.7) and integrating the resulting equation assuming $c_{s\infty} = \text{const}$ (see §§ 8 and 9), we obtain

$$a^2 = a_0^2 - \left(\frac{45}{4\pi}\right)^{1/2} \frac{B}{\rho_l} \left(\frac{\mathscr{D}_0}{\omega}\right)^{1/2} (c_{sb} - c_{s\infty})\, t, \tag{7.8}$$

where a_0 is the initial value of the particle radius. Denoting

$$K_* = \left(\frac{45}{4\pi}\right)^{1/2} B \left(\frac{\mathscr{D}_0}{\omega}\right)^{1/2} \frac{(c_{sb} - c_{s\infty})}{\rho_l}, \tag{7.9}$$

we rearrange (7.8) to the form

$$a^2 = a_0^2 - K_* t \tag{7.10}$$

which shows that the lifetime of a droplet or particle is given by

$$t_l = \frac{\rho_l a_0^2}{(45\mathscr{D}_0/(4\pi\omega))^{1/2} B(c_{sb} - c_{s\infty})}. \tag{7.11}$$

8. Vapour concentration, droplet temperature and liquid properties

The air/vapour mixture at the droplet surface can be assumed to be saturated since the phase-change process occurs at a rate which is much faster than the gas-phase transport processes. Therefore the equation of state of the products of evaporation may be written at the droplet surface as

$$\frac{p_{sat}}{c_{sb}} = \frac{R_g}{M} T_s, \tag{8.1}$$

where p_{sat} is the saturation pressure, R_g is the absolute gas constant, M is the molecular mass, and T_s is the surface temperature.

Liquid	Molecular mass M (g mole^{-1})	Density ρ_l (g cm^{-3})	Diffusion coefficient $\mathscr{D}_0$ (cm^2 s^{-1}),	Heat of evaporation I_v (kJ kg^{-1})
Methanol	32.042	0.792	0.159151	1189
Ethanol	46.068	0.789	0.121395	941
Propanol-2	60.096	0.785	0.101271	756
n-Heptane	100.198	0.684	0.069396	364
n-Octane	114.224	0.703	0.064598	359
n-Decane	142.276	0.730	0.057349	351

TABLE 3. Physical parameters of the liquids (Reid *et al.* 1987, and Fuller *et al.* 1966) at $t = 20\,^{\circ}\mathrm{C}$ and $p = 1024\,\mathrm{mbar}$.

The saturation pressure of several liquids is given as a function of the temperature by the Antoine equation (Reid, Prausnitz & Poling 1987)

$$p_{sat} = 0.001333224 \exp\left(A_* - \frac{B_*}{T_s + C_*}\right), \tag{8.2}$$

where p_{sat} is given in bar (1 bar $= 10^{-5}\,\mathrm{N\,m^{-2}}$), and T_s is taken in degrees Kelvin. The values of the parameters A_*, B_* and C_* for several liquids are shown in table 1. For water vapour at atmospheric pressure we use the following expression for the saturation pressure (Seaver *et al.* 1989):

$$p_{sat} = a_{0*} + T_s\left[a_{1*} + T_s\left(a_{2*} + T_s\{a_{3*} + T_s\left[a_{4*} + T_s\left(a_{5*} + a_{6*}T_s\right)\right]\}\right)\right], \tag{8.3}$$

where p_{sat} is given in mbar (1 mbar $= 10^2\,\mathrm{N\,m^{-2}}$) and T_s is taken in degrees Celsius. The values of the parameters a_{i*} are presented in table 2.

Knowing p_{sat} from (8.2) or (8.3), we find c_{sb} from (8.1) as

$$c_{sb} = \frac{p_{sat}(T_s)M}{R_g T_s}. \tag{8.4}$$

The physical parameters of the liquids involved in the calculations are listed in table 3. Their surface tension α is taken to be dependent on T_s according to the Hakim–Steinberg–Stiel equation (Reid *et al.* 1987). The equation

$$\alpha = D_* - E_* T_s \tag{8.5}$$

used in the calculations is a linear fit to the Hakim–Steinberg–Stiel equation. The surface tension α is given in g s^{-2}, and T_s is taken in degrees Celsius. The values of the parameters D_* and E_* are listed in table 1.

For water vapour at atmospheric pressure following Seaver *et al.* (1989) we take

$$\mathscr{D}_{0w} = 0.211\left(\frac{T_s + 273.15}{273.15}\right)^{1.94}, \tag{8.6a}$$

$$I_{vw} = 595.3 + T_s\left(0.483 + T_s \times 1.2 \times 10^{-3}\right), \tag{8.6b}$$

where the diffusion coefficient $\mathscr{D}_{0w}$ and the latent heat of evaporation for water I_{vw} (denoted by subscript w) are given in cm^2 s^{-1} and cal g^{-1}. The molecular mass, density and surface tension of water are taken as $M_w = 18.016\,\mathrm{g\,mol^{-1}}$, $\rho_{lw} = 1\,\mathrm{g\,cm^{-3}}$, and $\alpha = 72.74\,\mathrm{g\,s^{-2}}$, respectively.

For the thermal conductivity of air k_a used below we take (Seaver *et al.* 1989)

$$k_a = 5.8 \times 10^{-5} + 1.6 \times 10^{-7} T_s, \tag{8.7}$$

where k_a is given in cal cm^{-1} °C^{-1} s^{-1}, and T_s is in degrees Celsius.

We assume that water vapour may be present in air due to its humidity, and thus the water vapour concentration far from the droplet c_{sh} is given by

$$c_{sh} = \frac{p_\infty H M_w}{R_g T_\infty}, \tag{8.8}$$

where H is the relative humidity, and p_∞ and T_∞ are the pressure and temperature at infinity.

The surface temperature T_s is found from the thermal balance associated with the evaporation/condensation processes and heat removal from the droplet surface. Assuming that the water vapour from the surrounding air condenses at the droplet, we obtain the thermal balance in the form

$$\overline{\langle h_T \rangle}(T_\infty - T_s) = \overline{\langle h_c \rangle} \frac{p_{sat} M}{R_g T_s} I_v - \overline{\langle h_{cw} \rangle} \frac{p_\infty H M_w}{R_g T_\infty} I_{vw}, \tag{8.9}$$

where $\overline{\langle h_T \rangle}$, $\overline{\langle h_c \rangle}$ and $\overline{\langle h_{cw} \rangle}$ are the heat and mass transfer coefficients ($\overline{\langle h_c \rangle}$ for any vapour and $\overline{\langle h_{cw} \rangle}$ for water vapour). According to (7.4) we expect

$$\frac{\overline{\langle h_c \rangle}}{\overline{\langle h_T \rangle}} = \frac{\mathscr{D}_0}{k_a} \left(\frac{\kappa_0}{\mathscr{D}_0} \right)^{1/2}, \quad \frac{\overline{\langle h_{cw} \rangle}}{\overline{\langle h_T \rangle}} = \frac{\mathscr{D}_{0w}}{k_a} \left(\frac{\kappa_0}{\mathscr{D}_{0w}} \right)^{1/2}, \tag{8.10a, b}$$

where k_a and κ_0 are the thermal conductivity and diffusivity of air. Solving (8.9) for T_s and using (8.10a, b), we find

$$T_s = Y + \left[Y^2 - \left(\frac{\kappa_0}{\mathscr{D}_0} \right)^{1/2} \frac{\mathscr{D}_0 M I_v}{k_a R_g} p_{sat}(T_s) \right]^{1/2}, \tag{8.11a}$$

$$Y = \frac{1}{2} \left[T_\infty + \left(\frac{\kappa_0}{\mathscr{D}_{0w}} \right)^{1/2} \frac{\mathscr{D}_{0w} M_w I_{vw}}{k_a R_g} \frac{p_\infty H}{T_\infty} \right]. \tag{8.11b}$$

Equation (8.11a) is solved iteratively to find T_s. Note that in the case of evaporation of a water droplet, in (8.11a) $\mathscr{D}_0 = \mathscr{D}_{0w}$, $M = M_w$ and $I_v = I_{vw}$. Note also that given $\kappa_0 = 0.208$ cm^2 s^{-1} for air and the values of $\mathscr{D}_0$ from table 3 or $\mathscr{D}_{0w}$ from (8.6a), we can see that $0.918 \leqslant (\kappa_0/\mathscr{D}_0)^{1/2} \leqslant 1.9$ and the effect of this factor on the values of T_s is minor.

Due to the presence of the external toroidal vortices in the levitator space (the outer acoustic streaming flow; see figure 2c), the vapour concentration $c_{s\infty}$ at the outer boundary of the diffusion boundary layer at $t > 0$ may become different from its known initial value $c_{s\infty 0}$ (at $t = 0$) even for water droplets. Indeed, in the absence of external blowing, the vortices represent almost closed recirculation zones. Therefore the mass of vapour m_v increases in the vortices when the droplet evaporates. On the other hand, the external blowing of a gas jet into the vortices reduces the vapour mass there, since the gas displaces the vapour. Also diffusion from the vortices reduces the vapour concentration; thus

$$\frac{\mathrm{d}m_v}{\mathrm{d}t} = Q_m. \tag{8.12}$$

For an oblate droplet similarly to (7.7) the mass flow rate is given as

$$Q_m = -\frac{\mathrm{d}}{\mathrm{d}t}\left(\rho_l \tfrac{4}{3}\pi a^3\right) - (c_{s\infty} - c_{sh})\dot{V} - \frac{\mathscr{D}_0}{R_*}4\pi R_*^2(c_{s\infty} - c_{sh}). \tag{8.13}$$

Here a is the volume-equivalent droplet radius, $c_{s\infty}$ is the average vapour concentration in the vortices, which is assumed to be the same as that at the outer boundary of the diffusion boundary layer, and c_{sh} corresponds to the water vapour concentration in the gas jet due to humidity (given by (8.8)) when we consider evaporation of water droplets, otherwise (for other fluids) $c_{sh} = 0$; $\dot{V}$ is the rate of blowing; R_* is the effective radius of the vortices.

The first term on the right in (8.13) represents the vapour flux into the vortices due to droplet evaporation, the second is the vapour loss due to the external blowing, and the third is vapour loss due to diffusion. Also

$$m_v = c_{s\infty} L_*^3, \tag{8.14}$$

where L_*^3 is the volume of the vortices which is assumed to be approximately constant. Note that $R_* = (3/4\pi)^{1/3} L_*$.

Therefore from (8.12) to (8.14) we obtain the equation governing the time variation of $c_{s\infty}$ during droplet evaporation

$$L_*^3 \frac{\mathrm{d}c_{s\infty}}{\mathrm{d}t} = -\rho_l \tfrac{4}{3}\pi \frac{\mathrm{d}a^3}{\mathrm{d}t} - (c_{s\infty} - c_{sh})\dot{V} - \mathscr{D}_0 L_* (4\pi)^{2/3} 3^{1/3} (c_{s\infty} - c_{sh}). \tag{8.15}$$

The concentration $c_{s\infty}$ is subject to the initial condition

$$t = 0, \qquad c_{s\infty} = c_{s\infty 0}, \tag{8.16}$$

where $c_{s\infty 0}$ is the initial vapour concentration in the surrounding medium.

The simplified description of the mass transfer in the vortices outlined above is only a first sketch of the mass transfer there. A more accurate analysis might be based, in principle, on the Navier–Stokes equations, since $Re_s = O(1)$ (cf. the estimate of § 5, $Re_s = 2.35$). This, however, becomes too complicated given the sideways blowing into the vortices involved in the present work (see figure 4).

9. Numerical implementation, experimental procedure and comparison with experiments

9.1. *The main formulae*

From (6.31) and (6.33) we obtain the average Sherwood number in the form

$$\overline{\langle Sh\rangle} = K \frac{B}{\sqrt{\omega \mathscr{D}_0}}, \tag{9.1}$$

where

$$K = \frac{2}{\sqrt{\pi}} \frac{\overline{\left[|\langle \bar{u}_{1\infty}(\bar{x})\rangle| \bar{r}(\bar{x})\right]^{\langle \bar{u}_{1\infty}(\bar{x})\rangle / \langle \bar{\tilde{u}}_{1\infty}(\bar{x})\rangle}}}{\psi^{1/2}(\bar{x})} \left[\frac{\omega a/c_0}{A_{0e}/\left(\rho_0 c_0^2\right)}\right]^{1/2}, \tag{9.2a}$$

$$\psi(\bar{x}) = \int_{\bar{x}_2}^{\bar{x}} \left[\langle \bar{\tilde{u}}_{1\infty}(\bar{\xi})\rangle\right]^{-1} \left[|\langle \bar{u}_{1\infty}(\bar{\xi})\rangle| \bar{r}(\bar{\xi})\right]^{2\langle \bar{u}_{1\infty}(\bar{\xi})\rangle / \langle \bar{\tilde{u}}_{1\infty}(\bar{\xi})\rangle} \times \exp\left[-2\int_{\bar{x}}^{\bar{\xi}} \ln|\langle \bar{u}_{1\infty}\rangle \bar{r}| \frac{\mathrm{d}}{\mathrm{d}\bar{\eta}}\left(\frac{\langle \bar{u}_{1\infty}\rangle}{\langle \bar{\tilde{u}}_{1\infty}\rangle}\right) \mathrm{d}\bar{\eta}\right] \mathrm{d}\bar{\xi}. \tag{9.2b}$$

Here and hereinafter overbars mark dimensionless parameters: r, x, ξ and η are rendered dimensionless by an initial volume-equivalent droplet radius a_0, and $\langle u_{1\infty}\rangle$ by B; a is a current volume-equivalent dimensional radius of the droplet. The general overbar in (9.2a) denotes averaging over the droplet surface as in (6.33); $|\langle u_{1\infty}\rangle|$, etc. denote the corresponding magnitudes.

If the simplified formula (6.36) is used, K in (9.1) is given by

$$K = \frac{2}{\sqrt{\pi}} \frac{\overline{|\langle \bar{u}_{1\infty}\rangle|\bar{r}}}{\left[\int_{\bar{x}_2}^{\bar{x}} \langle \bar{u}_{1\infty}\rangle \bar{r}^2 \mathrm{d}\bar{x}\right]^{1/2}} \left[\frac{\omega a/c_0}{A_{0e}/\left(\rho_0 c_0^2\right)}\right]^{1/2}. \tag{9.3}$$

In the incompressible limit valid for small spherical droplets according to (7.4), the Sherwood number is given by (9.1) with

$$K = \left(\frac{45}{4\pi}\right)^{1/2} = 1.89. \tag{9.4}$$

The mass balance for an evaporating droplet is similar to (7.7), but with $Q_m = -4\pi a^2 \overline{\langle h\rangle}\,(c_{sb} - c_{s\infty})$, where $\overline{\langle h\rangle}$ is calculated via the Sherwood number (9.1). Therefore the mass balance (together with (8.15) and (8.16)) reduces to the system of differential equations

$$\frac{\mathrm{d}\bar{a}^2}{\mathrm{d}\bar{t}} = -K \left[\frac{A_{0e}/\left(\rho_0 c_0^2\right)}{\omega a_0/c_0}\right]^{1/2} \frac{(c_{sb} - c_{s\infty})}{(c_{sb} - c_{s\infty 0})} \left(\frac{B}{B_0}\right)^{1/2}, \tag{9.5a}$$

$$\frac{\mathrm{d}c_{s\infty}}{\mathrm{d}\bar{t}} = -2\pi \left(\frac{a_0}{L_*}\right)^3 \rho_l \left(\bar{a}^2\right)^{1/2} \frac{\mathrm{d}\bar{a}^2}{\mathrm{d}\bar{t}} - \left(\frac{1}{\tau} + \frac{1}{\tau_{\mathscr{D}}}\right)(c_{s\infty} - c_{sh}), \tag{9.5b}$$

$$\bar{t} = 0: \quad \bar{a}^2 = 1, \quad c_{s\infty} = c_{s\infty 0}, \tag{9.5c}$$

$$\tau^{-1} = \frac{\rho_l \dot{V}}{a_0^{3/2}(c_{sb} - c_{s\infty 0})\sqrt{B_0 \mathscr{D}_0}} \left(\frac{a_0}{L_*}\right)^3, \tag{9.5d}$$

$$\tau_{\mathscr{D}}^{-1} = \frac{\rho_l \mathscr{D}_0}{a_0^{1/2}} \frac{(4\pi)^{2/3} 3^{1/3}}{(c_{sb} - c_{s\infty 0})\sqrt{B_0 \mathscr{D}_0}} \left(\frac{a_0}{L_*}\right)^2. \tag{9.5e}$$

Here the equivalent droplet radius a is rendered dimensionless by its initial value a_0, t is rendered dimensionless by $\rho_l a_0^{3/2}/\left[(c_{sb} - c_{s\infty 0})\sqrt{B_0 \mathscr{D}_0}\right]$, where B_0 is the value of B corresponding to the SPL at $t = 0$ (the general case of variable SPL during droplet evaporation is discussed below).

In the case of sufficiently strong blowing when the dimensionless 'ventilation time' of the vortices τ tends to zero, the second term on the right in (9.5b) becomes dominant, and thus, integrating (9.5b), we obtain $c_{s\infty} = c_{sh} + (c_{s\infty 0} - c_{sh})\exp(-\bar{t}/\tau)$. Therefore, $c_{s\infty} \to c_{sh}$ since $\tau \to 0$. This means that in the case of strong blowing on an evaporating water droplet, the concentration $c_{s\infty} = c_{sh}$, which is the water vapour concentration in the gas jet due to humidity (cf. (8.8)). In the case of water droplets it can be also assumed that $c_{s\infty 0} = c_{sh}$. For any other liquid in the case of strong blowing $c_{s\infty} \to c_{sh} = c_{s\infty 0} = 0$. Therefore in the case of strong blowing $(c_{sb} - c_{s\infty})/(c_{sb} - c_{s\infty 0}) \equiv 1$, equation (9.5$b$) always becomes irrelevant, decoupling from (9.5a). Note also that the dimensionless 'diffusion time' $\tau_{\mathscr{D}}$ is assumed to be independent of the blowing rate.

If we assume (say, for the case $c_{sh} = c_{s\infty 0} = 0$) that vapour concentration variation is quasi-steady ($\mathrm{d}c_{s\infty}/\mathrm{d}\bar{t} = 0$), then (9.5*a*, *b*) yield

$$c_{s\infty} = c_{sb} \frac{Y_c}{Y_c + \left(c_{sb}/\rho_l\right)\left(\tau^{-1} + \tau_{\mathscr{D}}^{-1}\right)}, \tag{9.6a}$$

$$Y_c = 2\pi \left(\frac{a_0}{L_*}\right)^3 \left(\bar{a}^2\right)^{1/2} K \left[\frac{A_{0e}/\left(\rho_0 c_0^2\right)}{\omega a_0/c_0}\right]^{1/2} \left(\frac{B}{B_0}\right)^{1/2} \tag{9.6b}$$

which are used together with (9.5*a*) replacing equation (9.5*b*). It is seen that for sufficiently strong blowing when $\tau^{-1} \to \infty$, $c_{s\infty}$ according to (9.6*a*) tends to zero, which means that all the vapour is immediately blown off at the outer boundary of the acoustic boundary layer.

In the general case $K = K(\bar{a}^2)$ via (9.2), or via (9.3) if a simplified form (6.36) is used. In the incompressible limit $K = 1.89$, and (9.5*a*) can be integrated analytically (in the case of strong external blowing) yielding (7.8) to (7.10). To calculate K in (9.2) or (9.3) the boundary element method of YPT was used to compute the acoustic field p_{sr} and p_{si}, the droplet shape $r(z)$ (squeezed by the acoustic field) and the position L. This was done at every time step following the evolution of the droplet radius given by (9.5). Given the acoustic field around a levitated droplet, the acoustic streaming velocity $\langle u_{1\infty} \rangle$ was calculated from (4.20). Accounting for the expressions for A and A_1 in (4.9), one can deduce that the expression for $\langle u_{1\infty} \rangle$ in (4.20) involves the first and second derivatives of the acoustic field over the droplet surface, as well as the second derivatives of the functions determining the droplet shape. The derivatives were found numerically, and the results (especially for the second derivatives) were smoothed using the smoothing procedure from Hildebrand (1974, eq. (7.15.3) on p. 357).

In the following subsections, the experimental apparatus and technique used for the study of the evaporation behaviour of acoustically levitated pure liquid drops are described and a comparison of the experimental and theoretical results is given.

9.2. *Experimental procedure*

The theoretical work of the present paper is accompanied by an experimental investigation on the evaporation behaviour of acoustically levitated liquid droplets. For these experiments, the ultrasonic levitator already used by YPT was employed together with an image analysis system for determining the drop surface and volume as a function of time. The whole experimental apparatus is sketched in figure 4. The ultrasonic levitator supplied by Batelle Frankfurt (Germany) is characterized by the vibration frequency of the ultrasound transducer of 56 kHz. This frequency corresponds to the nominal sound wavelength $\lambda_0 = 0.61$ cm at an unperturbed air temperature $T_0 = 293$ K, where the unperturbed sound velocity in air $c_0 = 343.8\,\mathrm{m\,s^{-1}}$. It was shown in YPT that the harmonic content of the acoustic field in the levitator may be approximated safely by a single standing harmonic wave. The ultrasound waves are reflected from the concave surface of a round reflector plate positioned opposite the transducer at a distance of 1.6 cm, which is appropriate to allow the formation of five pressure nodes in this resonator. The distance between the transducer and the reflector can be adjusted accurately by means of a micrometer screw. The uncertainty in the reflector position is of the order of 20 μm. The relative positions of the transducer and reflector were kept constant throughout the measurements, and no active control of the sound pressure level (SPL) was applied.

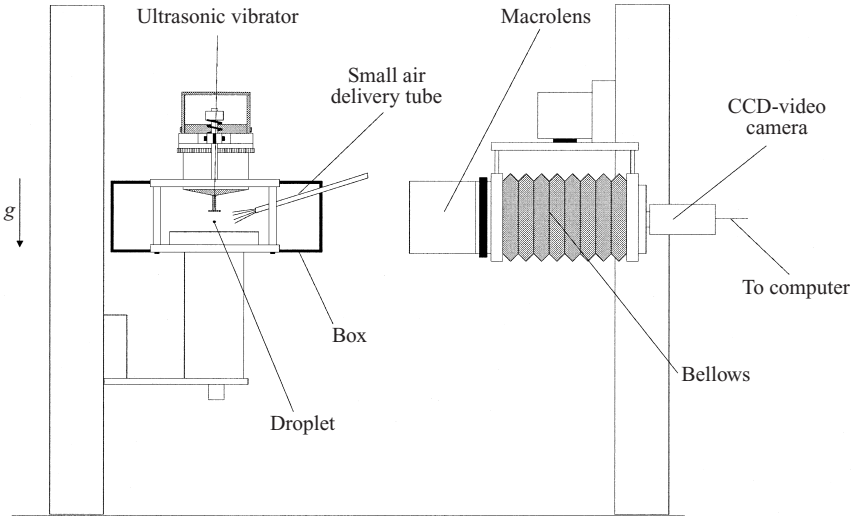

FIGURE 4. Sketch of the experimental setup for measuring the evaporation rate of acoustically levitated drops.

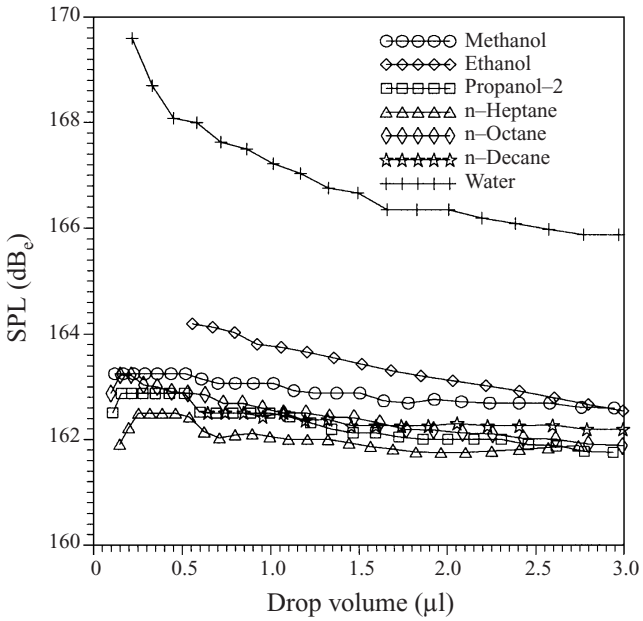

FIGURE 5. Computed evolution of the SPL during the evaporation process of drops of water, alcohols and alkanes in the acoustic field.

The droplets to be investigated are produced using a microlitre syringe. The drop volume may be chosen with an uncertainty of $\pm 0.05\,\mu$l. For producing the drop, the liquid is sucked into the syringe, and the volume of liquid representing the initial drop volume is pressed out of the syringe needle after it has been put close to the ultrasonic resonator. The drop is then inserted into the ultrasonic field, where the SPL had to be raised to the highest possible value for water drops to overcome the adhesion forces which attach the drop to the needle. After the subsequent adjustment of the

appropriate SPL at which the experiment is to be conducted, the drop is ready for the measurements. The SPL is determined from the aspect ratio of the drop shape for a given liquid and drop volume. The SPL changes with the aspect ratio and the volume of the drop during evaporation, as shown in figure 5. This evolution of the SPL is caused by the changing influence of the shrinking drop on the acoustic field. The relative positioning of the transducer and reflector of the levitator was slightly off-resonance in order to avoid disruption of the drops due to the high acoustic forces. The tuning of the levitator, however, changes due to the change in drop volume and shape.

For determining the evaporation behaviour, the drop volume is measured as a function of time using an imaging system. The particular parts of the system are a CCD video camera with macrolens and a PC equipped with a frame-grabber card and the software OPTIMAS. For imaging, the drop is illuminated from behind using a source of white light. The drop is imaged using a large magnification factor, which is calibrated before the measurement series by imaging a high-precision microscale etched on a glass plate. Based on this high-quality image of the drop, the image analysis software provides detailed information on the visible meridional cross-section of the drop. The data consist of the shape of an ellipse fitted to the drop contour, i.e. the lengths of the major and minor semiaxes s_l and s_s, the aspect ratio s_l/s_s of the ellipse and the location of the centre of the ellipse relative to the origin of a local coordinate system. Approximation of the cross-sectional shapes of the droplets levitated in the same levitator by oblate spheroids was shown to be rather accurate in YPT. In the present work the accuracy of such approximation has been better than 2% in the representation of the surface contour and around 2.5% in the representation of the drop volume. Based on these data, the volume of the spheroidal drop is computed via the equation $V_d = \frac{4}{3}\pi s_l^2 s_s$, assuming axial symmetry around the minor semiaxis. The surface S_{eo} of the (oblate) drop is given by the equation

$$S_{eo} = 2\pi s_l^2 \left(1 + \frac{s_s/s_l}{\sqrt{(s_l/s_s)^2 - 1}} \operatorname{arsinh} \sqrt{\left(\frac{s_l}{s_s}\right)^2 - 1} \right). \tag{9.7}$$

The geometric data are acquired at a frequency which may be chosen adequately for every evaporation behaviour. For doing this, a macro routine is used. All evaporation measurements were repeated three times to evaluate the scatter of the measured data. The data are further processed to compute the evaporation rate $\dot{m} = \rho_l 4\pi a^2 \mathrm{d}a/\mathrm{d}t$ on the basis of the volume-equivalent drop radius a and its derivative with respect to time as well as the surface of the drop as a function of time. This procedure is applicable only for pure liquid drops, where the density ρ_l of the drop liquid is constant and the drop mass can therefore be computed from its volume. For drops which consist of liquid mixtures, the drop mass must be determined by a weighing procedure which is much more time-consuming. A possible alternative for determining the drop mass may, however, be the evaluation of the position of the centre of gravity of the drop in the ultrasonic field, i.e. its displacement from a pressure node as a function of time during the evaporation process. Since the drop rises in the acoustic field as it loses mass, the displacement Δz_1 may be identified with the drop mass m via a calibration relation which yields the function $\Delta z_1 = f(m)$. This function is determined when using pure liquid drops.

For the present study, the evaporation behaviour of drops of water and a number of alcohols and alkanes was investigated for different initial drop volumes, sound pressure levels and ambient air temperatures and humidities. The initial drop volume

of 3 μl was chosen since it could be shown that the initial drop volume has no influence on the drop evaporation behaviour under the present experimental conditions with blowing.

In the experiment, blowing of dry air with relatively low and controllable humidity was possible. The levitator was confined in a box, and air was blown horizontally onto the levitated droplet from a small nozzle with the diameter $d_* = 0.39$ cm positioned at a distance $l_* = 7.0$ cm from the droplet. The volumetric flow rate of air $\dot{V}$ was varied from 0 (no blowing) to about 2 $\mathrm{l}_n\,\mathrm{min}^{-1}$ (standard litres per minute). At higher blowing rates stable levitation was impossible and the droplet was swept out from the acoustic field in a horizontal direction by the air stream. The air velocity at the nozzle exit $U_* = 4\dot{V}/(\pi d_*^2)$ thus varied in the range $0 \leqslant U_* \leqslant 279.1\,\mathrm{cm\,s}^{-1}$.

No direct measurement of the jet velocity field was made and thus some attempt has been made to estimate the velocity of the gas stream experienced by the droplet. The air flow produced by the nozzle can be characterized as a submerged gas jet with the exit Reynolds number of the order of 10^2. In spite of the beginning of transition to turbulence, such a jet can still be described rather accurately in terms of the Schlichting solution for the self-similar axisymmetric submerged laminar jet (Schlichting 1979). To find the velocity in the framework of the Schlichting self-similar solution, one needs to introduce a polar distance of the jet d_j. The maximal velocity in the jet cross-section u_{max} decreases along the jet axis as $u_{max} = \mathrm{const}/x_*$. At the nozzle exit (which corresponds to the polar distance from the jet origin) we thus have $U_* = \mathrm{const}/d_j$. Therefore the drop experiences the velocity

$$u_{max,\,drop} = \frac{\mathrm{const}}{l_* + d_j} = \frac{U_*}{l_*/d_j + 1}. \tag{9.8}$$

The momentum flux in the jet is equal to $\rho_0 U_*^2 \pi d_*^2/4$ and thus according to Schlichting (1979) the self-similar coordinate $\xi_{0.1}$ of the jet boundary $y_{0.1}$ (where, say, the longitudinal velocity is equal to $0.1u_{max}$) is given by

$$\xi_{0.1} = \left(\frac{3U_*^2 d_*^2}{64\nu_0^2}\right)^{1/2} \frac{y_{0.1}}{x_*}. \tag{9.9}$$

Using the longitudinal velocity profile in the jet given by Schlichting (1979), we obtain $0.1 = (1 + \xi_{0.1}^2/4)^{-2}$ and thus $\xi_{0.1} = 2.94$.

The nozzle circumference situated at $x_* = d_j$ and $y_* = d_*/2$ belongs to the boundary of the jet issued from the virtual pole. Therefore we obtain the polar distance d_j from (9.9) as

$$d_j = \left(\frac{3}{64}\right)^{1/2} \frac{U_* d_*^2}{2\nu_0} \frac{1}{2.94}, \tag{9.10}$$

and hence

$$\frac{l_*}{d_j} = \frac{2 \times 2.94(64/3)^{1/2}(l_*/d_*)}{U_* d_*/\nu_0}. \tag{9.11}$$

Taking, for example, blowing with $\dot{V} = 0.73\,\mathrm{l}_n\,\mathrm{min}^{-1}$, and thus $U_* = 101.85\,\mathrm{cm\,s}^{-1}$ we find from (9.11) for $l_* = 7.0\,\mathrm{cm}$, $d_* = 0.39\,\mathrm{cm}$ and $\nu_0 = 0.15\,\mathrm{cm}^2\,\mathrm{s}^{-1}$, that $l_*/d_j = 1.84$ and thus from (9.8) $u_{max,\,drop} = 35.85\,\mathrm{cm\,s}^{-1}$. This is the velocity of the gas stream impinging upon a levitated droplet.

However, a related velocity component $u_{acoust,bound}$ near the outer boundary of the acoustic boundary layer $y = \sqrt{2\nu_0/\omega}$ is much lower, since the acoustic boundary layer is situated near the bottom of that due to blowing. We find $u_{acoust,\,bound}$ assuming

a Blasius velocity profile resulting from blowing in the vicinity of the droplet. The self-similar coordinate of the Blasius profile given by Schlichting (1979) is $\eta = y(u_{max,drop}/(\nu_0 x))^{1/2}$. We should take x of the order of the droplet volume-equivalent radius $a \sim 10^{-1}$ cm. Thus for $u_{max,drop} = 35.85\,\mathrm{cm\,s^{-1}}$ we obtain $\eta \approx 0.045$. From the Blasius velocity profile we thus find $u_{acoust,bound}/u_{max,drop} \approx 0.664\eta = 0.03$. Therefore $u_{acoust,bound} = 1.07\,\mathrm{cm\,s^{-1}}$ which is significantly less than the smallest estimate for the acoustic streaming velocity $B_s = 3.52\,\mathrm{cm\,s^{-1}}$ (cf. § 5). Therefore we can conclude that at the blowing rate of $\dot{V} = 0.73\,\mathrm{l_n\,min^{-1}}$ the blowing effect on the vapour transport near the outer boundary layer is still negligible. It is definitely much smaller inside the acoustic boundary layer where the vapour transport is mainly due to the acoustic streaming.

On the other hand, a similar calculation for $\dot{V} = 2\mathrm{l_n\,min^{-1}}$ yields $U_* = 279.1\,\mathrm{cm\,s^{-1}}$, $u_{max,drop} = 166.9\,\mathrm{cm\,s^{-1}}$, and $u_{acoust,bound} = 10.8\,\mathrm{cm\,s^{-1}}$, which is already larger than the smallest streaming velocity $B_s = 3.52\,\mathrm{cm\,s^{-1}}$. Therefore for such blowing velocity the related convective effects begin to dominate the acoustic transport of vapour.

The boundaries between the regimes where blowing has no effect on the droplet evaporation in the acoustic field, where it has an effect mainly on vapour concentration outside the acoustic transport area, and where the blowing dominates the vapour transport process were established in the experiments. The results are discussed in § 9.3 below.

As a practical aspect of the experiments it should be noted that it is virtually impossible to begin with a droplet of a prescribed volume. Typically one begins an experiment with a droplet volume 10% larger than the nominal, follows the volume decrease, and starts recording the data from the desired volume. Since, during the evaporation of the portion of the drop in excess of the desired initial volume, continuous ventilation of the toroidal vortices is applied, a constant (low) humidity of the gaseous environment of the drop is maintained all the time. Nevertheless, due to the above procedure some uncontrollable vapour concentration in the vortices might be present at the instant when the measurements begin.

9.3. *Comparison of theoretical and experimental results*

The sound pressure level SPL in the levitator was established using the procedure developed in YPT. It allows one to find the effective pressure amplitude of the incident acoustic field A_{0e} from a measured aspect ratio s_l/s_s of a levitated droplet. The SPL is found as in YPT using the definition

$$\mathrm{SPL} = 20\log_{10}(A_{0e}) + 74, \tag{9.12}$$

where A_{0e} is in dyne cm^{-2}. The SPL found from (9.12) is denoted in the present work by $\mathrm{dB_e}$ as in YPT. If one wishes to define the SPL using the root-mean-square pressure amplitude $p_{rms} = A_{0e}/\sqrt{2}$ in (9.12) instead of A_{0e}, the SPL will be lower than the value in $\mathrm{dB_e}$ by 3.01 decibels.

Note that the method of YPT for SPL calibration is subject to an error when air blowing is involved, since the latter results in an additional droplet squeezing and thus affects the axis ratio. The additional droplet squeezing due to blowing, however, was not large, and thus the calibration of the acoustic field was still accurate, as the comparison of the predictions with experimental data shows below.

The experiments showed that droplet evaporation is accompanied by a variation of the aspect ratio. Therefore it turned out that the SPL increases during droplet evaporation. This result is actually anticipated, since it is known that the presence of a large squeezed droplet in a levitator results in a resonance shift caused by scattering

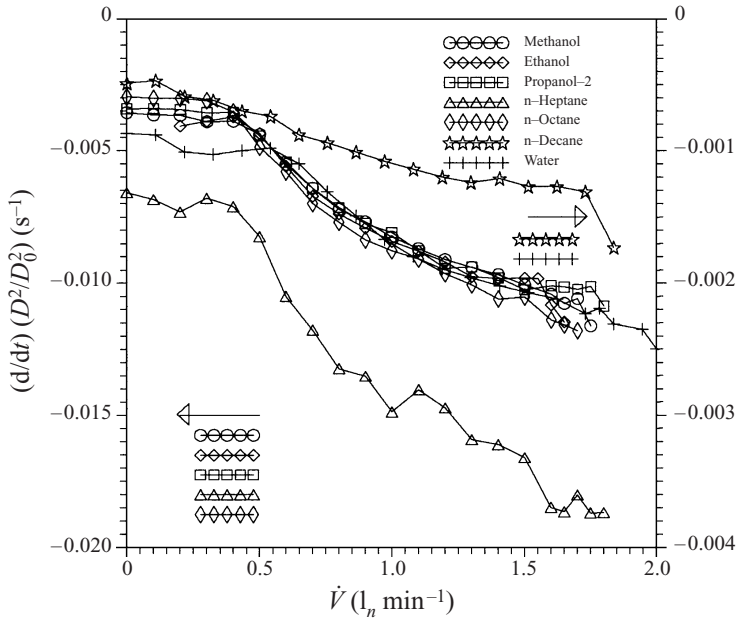

FIGURE 6. The slopes of the D^2 curves for water, alcohol and alkane drops with an initial volume of 3 µl as functions of the blowing rate of air.

(Trinh & Hsu 1986). When a droplet becomes smaller in the course of evaporation, the levitator tends back to the resonance conditions and thus the SPL increases.

The computation of the SPL for each aspect ratio during the lifetime of the drop yielded the function SPL $= f(V)$, depending on the drop volume V. It is emphasized that such a calibration has been done for all the liquids independently to account for the effect of liquid physical parameters (e.g. of the surface tension). Figure 5 shows the computed functions for water, alcohol and alkane drops, which could be verified by measurements of the SPL with a piezoelectric pick-up. As a consequence of this result, the SPL was treated as variable with time in the evaporation computations.

Before going into the details of the measurement series, the influence of the ventilation of the toroidal vortices by blowing of dry air was investigated. The drop evaporation, characterized by the time-average slope $(\mathrm{d}/\mathrm{d}t)(D^2/D_0^2)$ of the curve $D^2/D_0^2 = f(t)$, which is the derivative of the normalized drop surface with respect to time, was measured as a function of the volumetric flow rate of the blowing air for all liquids under investigation. Figure 6 depicts the results for water, alcohol and alkane drops with an initial volume of 3 µl at the initial values of the SPL corresponding to the extreme right-hand points in figure 5. It can be seen from the results in figure 6 that the drop evaporation behaviour is affected by the blowing in a range of air volumetric flow rates $\dot{V}$ between e.g. 0.5 and 1.6 l_n min^{-1} for water and between 0.4 and 1.4 l_n min^{-1} for ethanol. Actually two plateaux are clearly visible in figure 6. For small $\dot{V}$ (up to about 0.4 to 0.5 l_n min^{-1}) no influence of the sideways blowing on the drop evaporation is seen. Also at $\dot{V}$ from about 1.4 l_n min^{-1} to about 1.8 l_n min^{-1} there is practically no effect of blowing for all the liquids except the case of n-heptane (where the droplet position might be unstable due to interaction of blowing and levitation since n-heptane is the least dense liquid used). At intermediate values of $\dot{V}$ ($0.4 \leqslant \dot{V} \leqslant 1.4\,\mathrm{l}_n\,\mathrm{min}^{-1}$) evaporation is influenced by blowing. This presumably

results in a permanent reduction of the vapour concentration at the outer boundary of the acoustic boundary layer $c_{s\infty}$. At very large values of $\dot{V}$ above 1.8 l_n min^{-1} the blowing-driven (convective) evaporation becomes evident, and the evaporation rate begins to increase drastically.

One of the most important conclusions following from figure 6 is the fact that the evaporation rate practically does not change at the second plateau $1.4 \leqslant \dot{V} \leqslant 1.6 l_n$ min^{-1} in spite of the variation of the blowing rate. This is explained by the 'saturation' of the vapour concentration $c_{s\infty}$ at zero level, as foreseen from (9.6*b*) for sufficiently strong blowing. Therefore we expect that the experimental data obtained in this range of $\dot{V}$ might be described substituting in (9.5*a*) $c_{s\infty} = c_{sh}$ for water and $c_{s\infty} = 0$ for the other liquids. This has been done in the present work leading to the results discussed below. Note also that the experiments described below were all carried out at the conditions of ventilated vortices, corresponding to the second plateau, i.e. at a constant liquid vapour concentration in the ambient air, which is approximately zero for the alcohols and alkanes, and given by the controlled humidity of the blowing air for water.

As mentioned above, at $\dot{V} \geqslant 1.8$ l_n min^{-1} the air velocity experienced by the droplet becomes so high that the evaporation approaches the convection-driven regime. However, blowing in this range tends to blow out the droplets from the levitator in a radial direction, so that a stable levitation is no longer possible. This means that under the conditions of stable levitation we were able to investigate only evaporation driven by the acoustic streaming, and we were unable to achieve the convection-driven evaporation in the levitator due to the blow out of the droplet.

The image processing system used for the experiments allowed measurements of the shape of the meridional section of the spheroidal drop to be performed. The shapes at the instant when evaporation starts are depicted in figures 7(*a*) to 7(*g*) for the liquids listed in table 3 and for water. The values of the sound pressure level at this condition were mentioned above. The results show very good agreement between the computed and the measured results.

The aspect ratios of the drop shapes as functions of time, measured and computed, are depicted in figures 8(*a*) to 8(*g*) for the seven liquids investigated here; results of a computation with constant SPL are also shown. Since the variation of the SPL with time was determined computationally according to the measured evolution of the aspect ratio of the drop using the procedure of YPT discussed above, it is not surprising that the aspect ratio computed with variable SPL and the measured data are in very good agreement, while the data computed with constant SPL (the initial value) predict far smaller deformations of the drop than measured in the experiments.

Figures 9(*a*) to 9(*g*) show the measured evaporation behaviour of droplets of the seven liquids investigated with an initial volume of 3 µl, represented by the decrease of the normalized drop surface with time. The measured data are represented by the filled symbols. For comparison, two curves computed using the present theory are also given in the figure. The curves marked by the open circles show the results of computations with the SPL kept constant at its initial value. The curves marked by the open squares show the data computed with variable SPL. The good agreement between these latter curves and the measured data is clearly visible, indicating the correct representation of the evaporation process by the present theory.

Figure 10 shows the measured displacement of the drop centres from the nearest pressure node as a function of time for drops of the liquids considered here with an initial volume of 3 µl. Again the measured data agree better with the results of the computation with variable SPL. The results show the rise of the drops in the acoustic

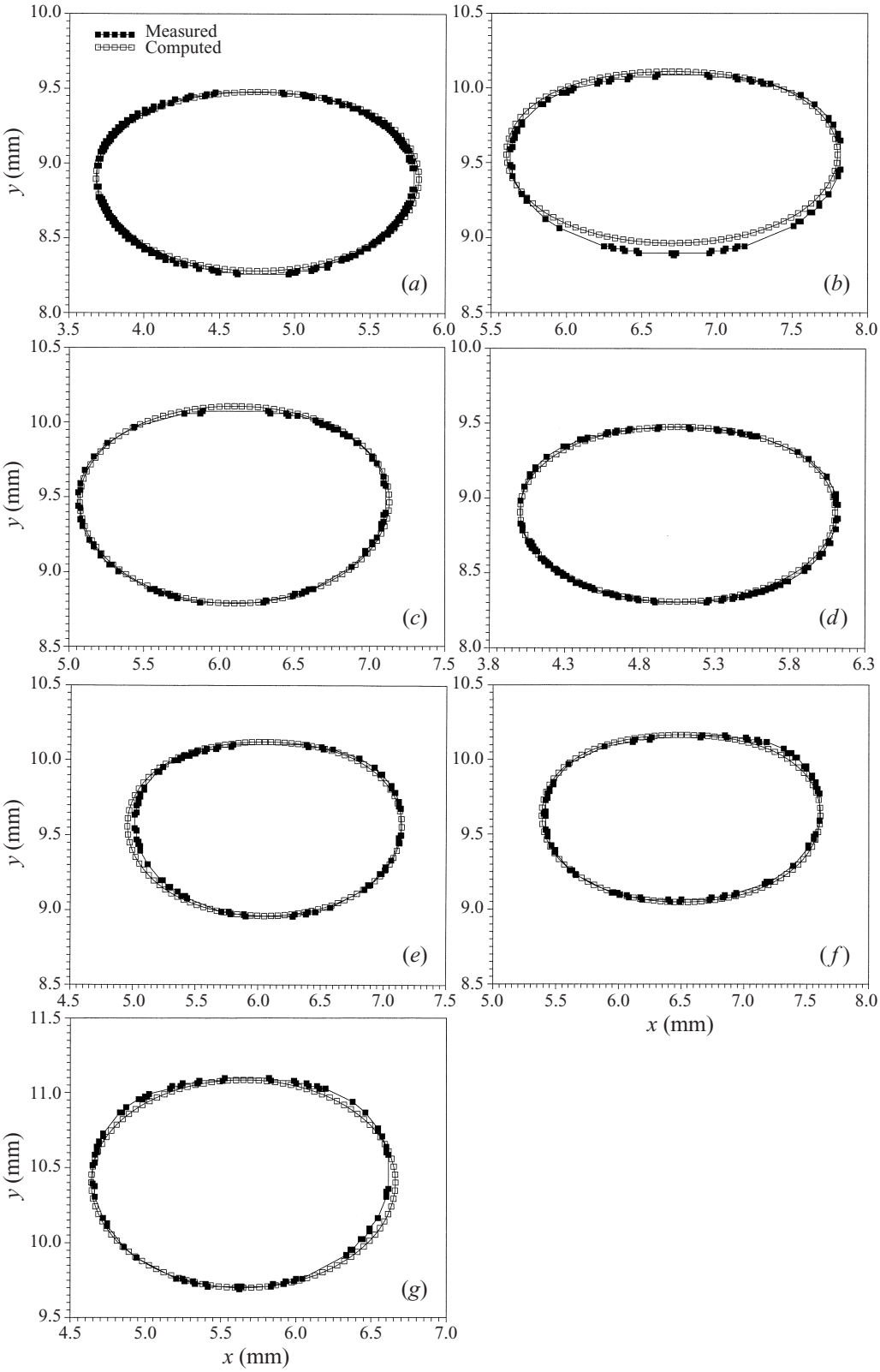

FIGURE 7. For caption see facing page.

field during the evaporation process. Since the experimental data exhibit only very small scatter, they are suitable for determining the drop mass from the displacement. This is of great interest for determining the evaporation rate of drops in the second drying stage of suspensions, dispersions and liquid mixtures. Note also that the displacement value is the most sensitive parameter in the acoustic levitation as was shown in YPT. It may be affected by small droplet displacements from the levitator axis in the horizontal direction due to the blowing. These horizontal displacements may initiate three-dimensional effects in the acoustic field, which immediately affect such sensitive characteristics as the vertical displacement from the pressure node.

The relevant characteristic number for quantifying the mass transfer is the Sherwood number $\overline{\langle Sh\rangle}$. This number is determined by the coefficient K in equation (9.1), together with the velocity B determined by the SPL via (2.2) and (9.12). It has been shown in § 7 that the value of K converges to 1.89 as the drop size decreases and the drop becomes more and more spherical. In figure 11(a, b) the temporal evolution of the computed value of K is shown together with the asymptote 1.89. The values of K decrease with time, i.e. with decreasing drop surface. The results show that the values of K are significantly larger than 1.89 at the beginning when the droplet is still large and squeezed. Only near the point of extinction, when the droplet becomes small due to evaporation, do the values of K approach 1.89.

It is emphasized that, for calculating $\overline{\langle Sh\rangle}$ from equation (9.1), we find A_{0e} and B from a given SPL via (9.12) and (2.2). If one uses the same value of the SPL, but defined via the root-mean-square of the pressure amplitude ($p_{rms} = A_{0e}/\sqrt{2}$ instead of A_{0e} in (9.12)), then

$$B_{rms} = B\sqrt{2}, \qquad K_{rms} = \frac{K}{\sqrt{2}} \tag{9.13}$$

appear in all the formulae. Therefore, for small spherical droplets (9.1) and (9.4) may be rearranged into

$$\overline{\langle Sh\rangle} = 1.336\frac{B_{rms}}{\sqrt{\omega\mathscr{D}_0}} \tag{9.14}$$

(since $\sqrt{45/(4\pi)}/\sqrt{2} = 1.336$). Expression (9.14) may also be rearranged to the form

$$\overline{\langle Sh\rangle} = 1.336\left(\frac{v_0}{\mathscr{D}_0}\right)^{1/2}\frac{B_{rms}}{\sqrt{\omega v_0}} \tag{9.15}$$

which should be compared with the approximation proposed in Gopinath & Mills (1993) for the results of their numerical calculations of heat transfer from a sphere due to the acoustic streaming

$$\overline{\langle Sh\rangle} = 1.314\left(\frac{v_0}{\mathscr{D}_0}\right)^{0.665}\frac{B_{rms}}{\sqrt{\omega v_0}} \quad \text{for } 0.1 \leqslant \frac{v_0}{\mathscr{D}_0} \leqslant 10.0. \tag{9.16}$$

(Following Tian & Apfel (1996) we put the results of Gopinath & Mills (1993) for $\overline{\langle Nu\rangle}$ into the expression (9.16) for $\overline{\langle Sh\rangle}$). Expression (9.16) is valid for $B_{rms}/\sqrt{\omega v_0} \gg 1$, which is identical to $(B_{rms}/\omega a)\sqrt{Re} \gg 1$ according to (2.1). In our case, as was shown in § 2, $Re \sim 2.3 \times 10^4$, whereas $(B_{rms}/\omega a) \sim 10^{-2}$. Therefore in our case $B_{rms}/\sqrt{\omega v_0}$

FIGURE 7. The shapes of (*a*) methanol, (*b*) ethanol, (*c*) propanol-2, (*d*) n-heptane, (*e*) n-octane, (*f*) n-decane and (*g*) water droplets with an initial volume of 3 µl computed and measured by means of the image processing system. The SPL is 162.591, 162.531, 161.747, 161.872, 161.872, 162.184 and 165.875 dB_e for the seven liquids, respectively. Blowing rate $\dot{V} = 1.4\,\mathrm{l}_n\,\mathrm{min}^{-1}$.

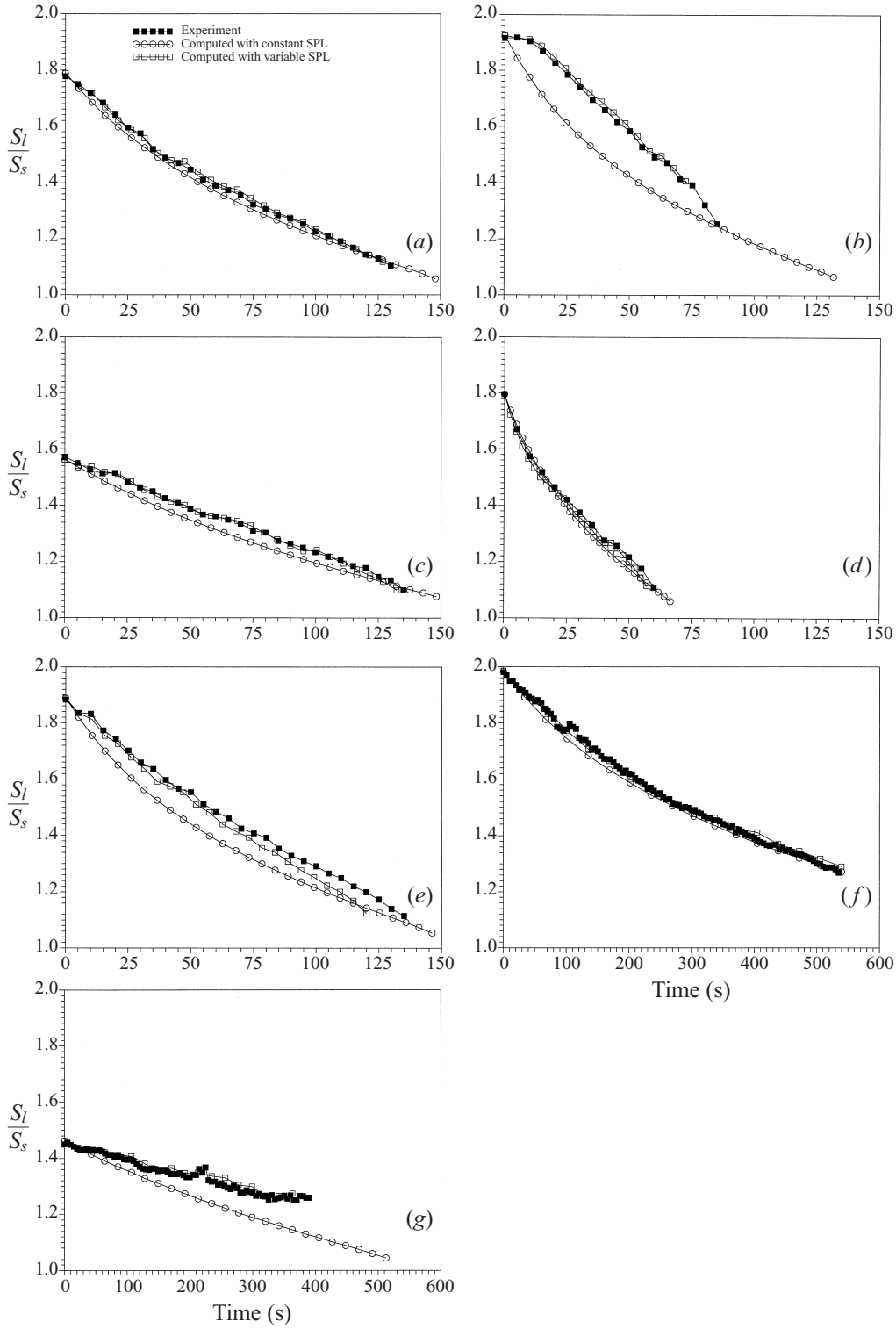

FIGURE 8. For caption see facing page.

is of the order of several units and the condition of applicability of approximation (9.16) is approximately satisfied. Comparison of (9.15) with (9.16) shows that they predict similar values of the Sherwood number.

Expression (9.14) is compared in figure 12 with the experimental data of Burdukov & Nakoryakov (1965*b*) and Gopinath & Mills (1993). The former positioned metal spheres covered by a solid camphor layer in acoustic fields of various intensities (SPL = 150 to 163 dB) and frequencies ($11.5 \times 2\pi$ to $18 \times 2\pi$ kHz) and measured the mass transfer rate due to camphor sublimation. The latter put a thermistor bead in an acoustic field of SPL = 155 dB and frequency of 1018 Hz and measured the heat transfer rate. Actually they measured $\overline{\langle Nu \rangle}$. In the present paper we refer to their result as $\overline{\langle Sh \rangle}$.

In figure 12 the dotted straight line corresponding to (9.14) is valid for small spherical bodies ($\Omega \ll 1$). It is seen, however, that it fits pretty well the data of Burdukov & Nakoryakov (1965*b*) obtained for spheres with $\Omega \leqslant 1$. The dashed curve shows the numerical results for big 5 µl n-hexadecane droplets ($\rho_l = 0.7734\,\mathrm{g\,cm^{-3}}$, $\alpha = 27.64\,\mathrm{g\,s^{-2}}$) corresponding to the beginning of their evaporation ($t = 0$). These droplets are squeezed significantly by the acoustic field. As a result, the corresponding values of the Sherwood number are higher than those predicted by (9.14) (cf. figure 11).

As follows from figure 12, (9.14) represents a good approximation for spherical bodies positioned at the pressure node, even if they are not small enough to make the incompressible approximation formally valid. To check this, we computed the evaporation process of a levitated 5 µl droplet of an artificially low density ($\rho_l = 0.01\,\mathrm{g\,cm^{-3}}$), and high surface tension ($\alpha = 200\,\mathrm{g\,s^{-2}}$). The value of K changed with time in the range from about 2.1 to 1.89, which is close to the predictions of the incompressible approximation (9.4) and (9.14), in spite of the fact that the droplet size is comparable with the sound wavelength ($\Omega = 1.0978$). However, this artificial droplet was practically spherical and positioned close to the pressure node, which seems to be enough to apply (9.4) and (9.14). Therefore the deviation of the dashed curve in figure 12 may be attributed to significant droplet squeezing by the acoustic field.

For mass transfer from a sphere subject to a relatively strong forced convection, the Sherwood number is given by

$$\overline{\langle Sh \rangle} \sim Re_c^{1/2} Sc^{1/3}, \tag{9.17}$$

where $Re_c = V_c a/\nu_0$ is the convective Reynolds number based on a velocity V_c, and $Sc = \nu_0/\mathscr{D}_0$ is the Schmidt number (Bird *et al.* 1960, p. 647). In the present case the flow at the outer boundary of the acoustic boundary layer is mainly associated with the acoustic streaming. Thus taking $V_c \sim B_s \sim B_{rms}^2/(\omega a)$ (cf. (5.19)), we obtain from (9.17)

$$\overline{\langle Sh \rangle} \sim \left(\frac{\nu_0}{\mathscr{D}_0}\right)^{1/3} \frac{B_{rms}}{\sqrt{\omega \nu_0}} \tag{9.18}$$

which is rather close to (9.15) and (9.16), especially given $\nu_0/\mathscr{D}_0 = O(1)$. (A similar approximation was used in Lee & Wang (1988) to estimate the Nusselt number in the acoustic field).

FIGURE 8. Temporal evolution of the aspect ratio s_l/s_s of drops of (*a*) methanol, (*b*) ethanol, (*c*) propanol-2, (*d*) n-heptane, (*e*) n-octane, (*f*) n-decane and (*g*) water with an initial volume of 3 µl. The data computed with variable SPL agree well with the measurements. The results marked as 'computed with constant SPL' were computed at the values of SPL corresponding to $t = 0$, when the droplet volumes were 3 µl. Blowing rate $1.4\,\mathrm{l_n\,min^{-1}}$.

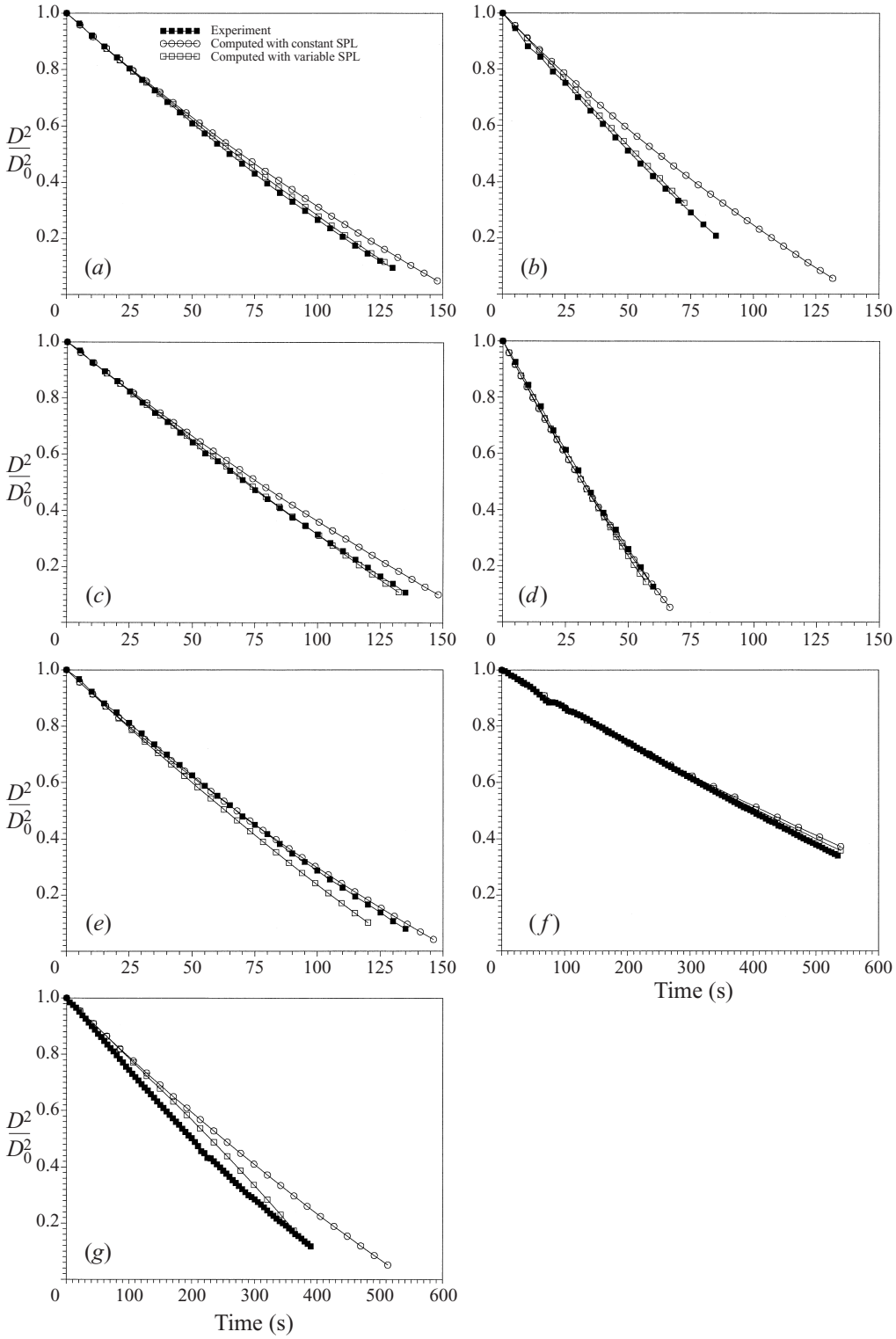

FIGURE 9. For caption see facing page.

The Sherwood numbers computed on the basis of the present theory for drops with initial volumes of 3 μl are shown as functions of time in figure 13 for the liquids discussed here. It is seen from these results that the Sherwood number is far from the value of 2 for purely diffusive mass transfer (without the acoustic field and blowing). We may conclude from this fact that an acoustic levitator with a strong acoustic field is not suitable for investigating diffusive heat and mass transfer from the levitated drops. In contrast to this, Seaver *et al.* (1989) and Tian & Apfel (1996) claimed that the effect of the acoustic field on droplet evaporation is negligible and that mass transfer is driven purely by molecular diffusion of the vapour. In that case, $Sh = 2$, and a single equation describing the evolution of the droplet radius is readily available

$$\frac{\mathrm{d}}{\mathrm{d}t}\left(4\pi a^2\right) = -\frac{8\pi \mathscr{D}_0 M}{\rho_l R_g}\left(\frac{p_{sat}}{T_s} - \frac{p_{v\infty}}{T_\infty}\right), \tag{9.19}$$

where $p_{v\infty}$ is the vapour pressure far from the droplet. The above authors claimed that equation (9.19) described their data for drop evaporation in the acoustic field. Note, however, that Tian & Apfel (1996) worked with a field with SPL from 140 to 150 dB. Also, Seaver *et al.* (1989) worked with a field with SPL $\approx$ 150 dB. So their fields were weak and their droplets were small compared to those of the present work where the effect of the acoustic field is found to be significant. The fact that $\overline{\langle Sh \rangle}$ is a growing function of SPL according to the experimental data of Burdukov & Nakoryakov (1965*b*) shown in figure 12 also supports the conclusion that the effect of the acoustic field on droplet evaporation may be strong. Also it should be added that Seaver & Peele (1990) reported that equation (9.19) does not describe their experimental data as perfectly as reported by Seaver *et al.* (1989).

Equation (9.19) may be rewritten using (8.4) as

$$\frac{\mathrm{d}a^2}{\mathrm{d}t} = -\frac{2\mathscr{D}_0}{\rho_l}\left(c_{sb} - c_{sh}\right) \tag{9.20}$$

which in the integrated form yields the lifetime of a droplet

$$t_l = \frac{\rho_l a_0^2}{2\mathscr{D}_0\left(c_{sb} - c_{sh}\right)}. \tag{9.21}$$

For the data corresponding to the present experiments (even without blowing when the lifetime is maximal), equation (9.21) may underestimate or overestimate the measured lifetime by about 100%. For example, for methanol, equation (9.21) yields $t_l \approx 100$ s instead of the measured (without blowing) $t_l = 265$ s, whereas for propanol-2 it predicts $t_l = 600$ s instead of the measured value (without blowing) of $t_l = 330$ s. These estimates show additionally that the description based on the model assuming purely diffusional transport fails.

Analytical results for the distributions of the acoustic streaming velocity $\langle \bar{u}_{1\infty} \rangle$ and the Sherwood number $\langle Sh \rangle$, valid only for very small droplets, are obtained from (5.18) and (7.3). These results are compared with the numerical ones based on (4.20) and (6.31) in figures 14(*a*) to 14(*e*). It is seen that the asymptotical analytical results approach the numerical ones only for droplets with volumes less than about 0.01 μl

FIGURE 9. Temporal evolution of the normalized drop surface for (*a*) methanol, (*b*) ethanol, (*c*) propanol-2, (*d*) n-heptane, (*e*) n-octane, (*f*) n-decane and (*g*) water droplets with an initial volume of 3 μl and initial SPL of 162.591, 162.531, 161.747, 161.872, 161.872, 162.184 and 165.875dB$_e$, respectively. The vapour concentration in the toroidal vortices is kept constant (close to zero for water, and zero for the other liquids) by ventilation. Blowing rate 1.4 l$_n$ min^{-1}.

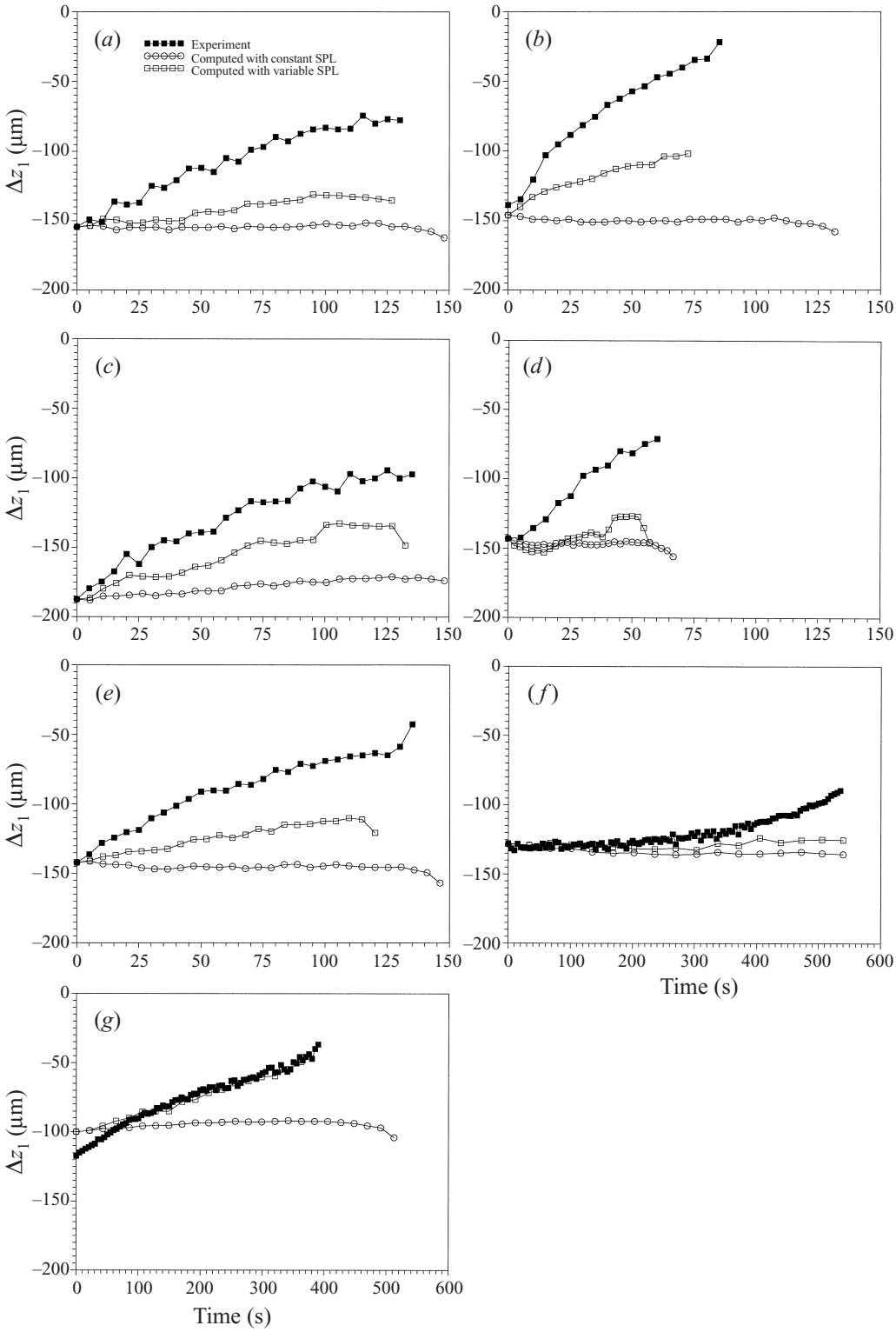

FIGURE 10. For caption see facing page.

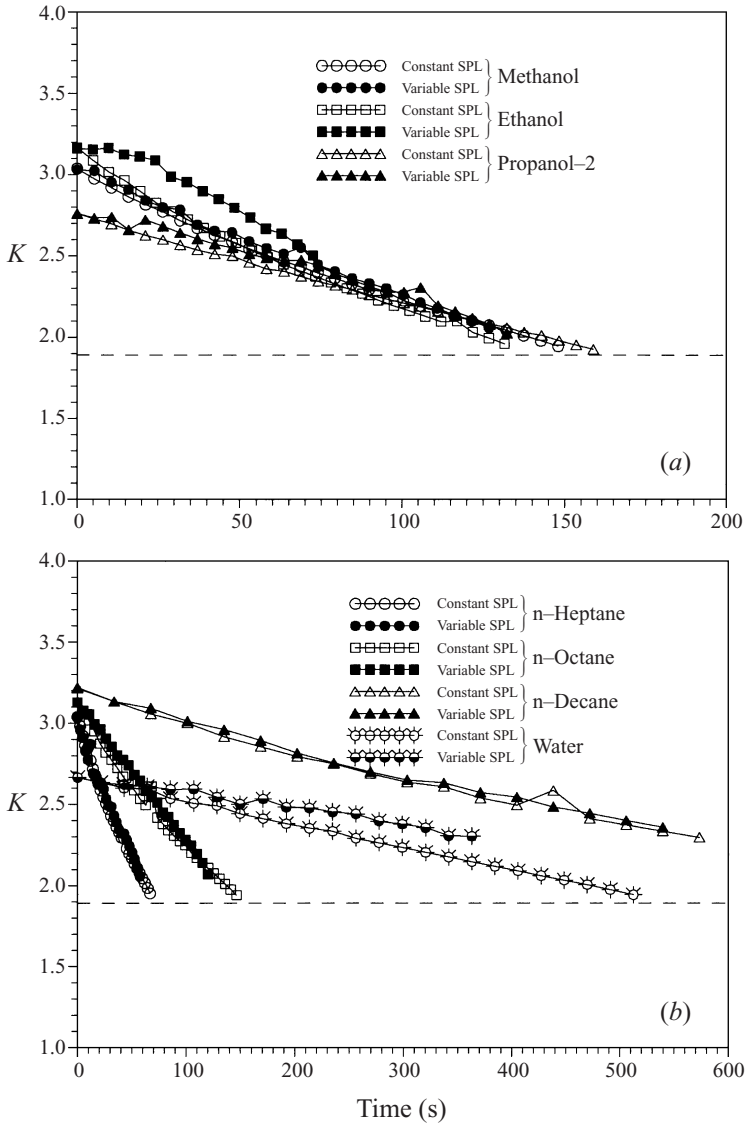

FIGURE 11. Temporal evolution of computed values of the coefficient K in equation (9.1) (*a*) methanol, ethanol and propanol-2 droplets and (*b*) n-heptane, n-octane, n-decane and water droplets with the initial volume of 3 µl. The SPL increases with time and leads to larger values of K than those at a constant SPL.

($a_0 \leqslant 0.0134$ cm). For droplets with $a_0 > 0.0134$ cm the incompressible approximation fails (also their squeezing may become important) and the Sherwood number may be described accurately only using (9.1) with (9.2) or (9.3).

FIGURE 10. Displacement of the centres of evaporating (*a*) methanol, (*b*) ethanol, (*c*) propanol-2, (*d*) n-heptane, (*e*) n-octane, (*f*) n-decane and (*g*) water drops from the nearest pressure node as functions of time for the initial drop volume of 3 µl. Experiments with ventilation of the vortices. Blowing rate 1.4 l_n min^{-1}.

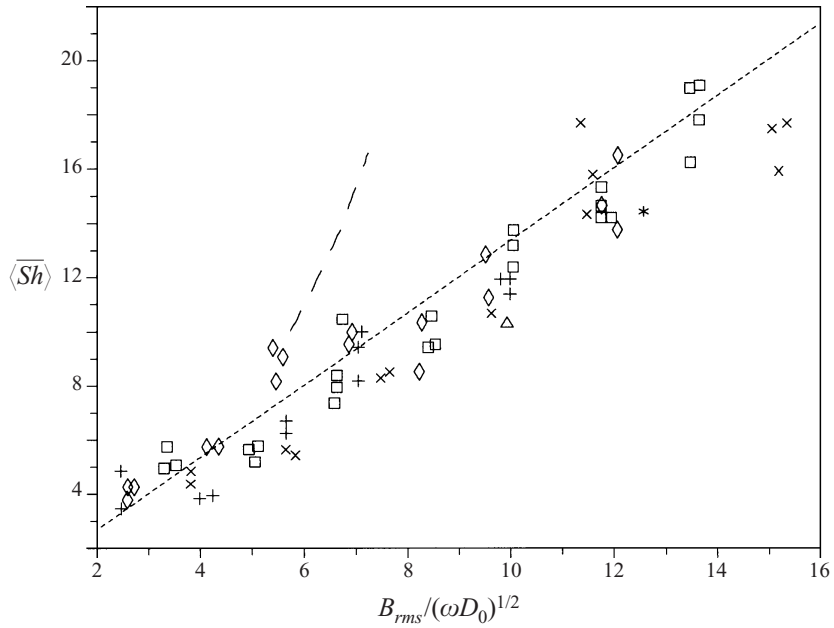

FIGURE 12. Comparison of the results from various experiments with the present calculations. The experimental data of Burdukov & Nakoryakov (1965*b*) are represented by symbols corresponding to the following frequencies in kHz and sphere diameters in mm: ◇, (18 × 2π, 6); +, (18 × 2π, 3.5); □, (11.5 × 2π, 10); ×, (11.5 × 2π, 6); △, (11.5 × 2π, 3.5). * Corresponds to the experimental result of Gopinath & Mills (1993). The dotted straight line corresponds to (9.14), formally valid for small spherical bodies. The dashed curve shows the numerical results for big 5 μl n-hexadecane droplets squeezed by the acoustic field.

10. Conclusion

A theoretical description of the ultrasonic field around an acoustically levitated liquid drop and its influence on heat and mass transfer between the drop and the ambient air is given. The theory is applicable to drops of arbitrary size relative to the sound wavelength, including those of the order of the wavelength, where the compressibility of the gas flow cannot be ignored. It is emphasized that, to our knowledge, the theory represents a first description of the compressible acoustic streaming and its effect on heat and mass transfer. The theory also accounts for droplet squeezing by the acoustic field.

The essential results of the theory are the drop shape, as well as the evaporation rate of the drop as functions of time. Furthermore, the location of the drop in the acoustic field, i.e. its displacement from a pressure node, and the temporal evolution of the Sherwood or Nusselt numbers are computed.

A qualitatively new effect revealed in the present work is the existence of the first and second plateaux in the droplet evaporation rate, where radial blowing of air towards the drop does not affect evaporation at all. Also the role of ventilation of the toroidal vortices about the levitated droplet and its effect on vapour concentration and evaporation rate have been elucidated. The existence of the acoustically driven evaporation processes has been unambiguously shown. The effect of the acoustic field on droplet evaporation appears to be related to the acoustic streaming and squeezing of the drops by the acoustic radiation pressure. In strong fields this effect becomes dominant, which makes it impossible to study convective heat and mass transfer using

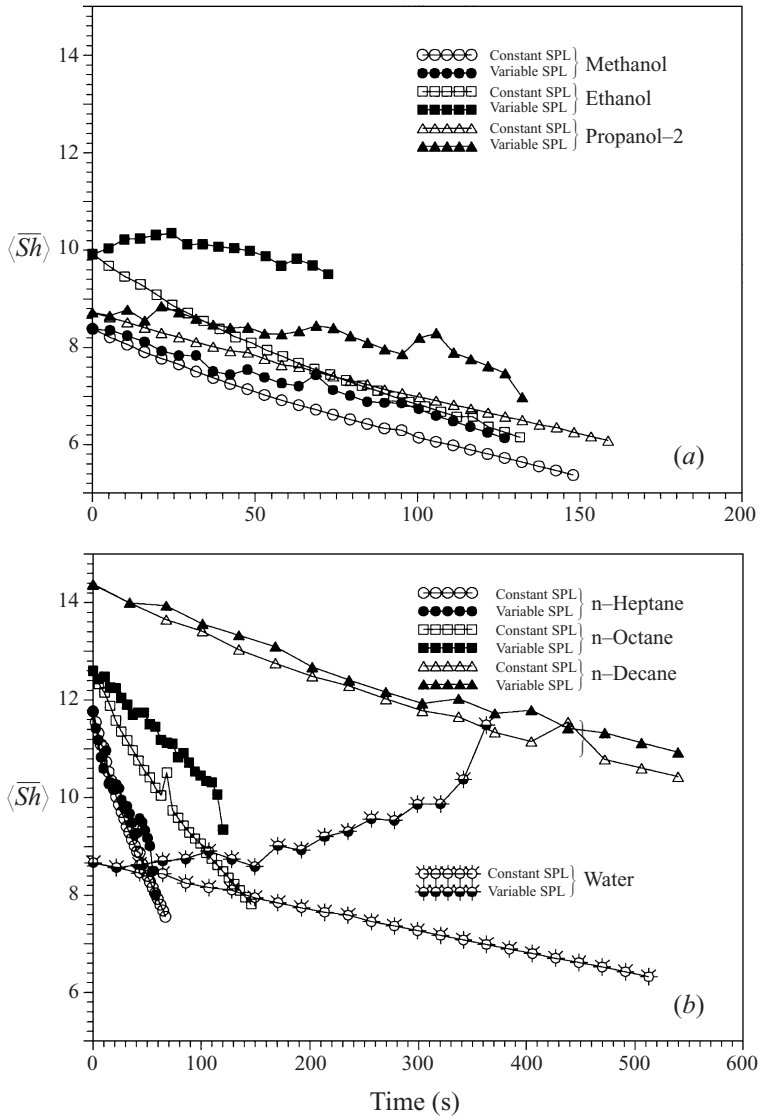

FIGURE 13. The Sherwood numbers for (*a*) methanol, ethanol and propanol-2 droplets and (*b*) n-heptane, n-octane, n-decane and water droplets with the initial volume of 3 µl as functions of time. Computations with constant and variable SPL. All values are larger than 2. Data obtained with variable SPL for water show an increase of $\overline{\langle Sh\rangle}$ with time.

droplets levitated in strong acoustic fields since this 'non-intrusive' technique actually becomes very intrusive.

Acoustically driven evaporation rates of seven liquids including water, alcohols and alkanes were measured. Comparison of the theoretical predictions with the experimental data for evaporating drops in the ultrasonic levitator shows good agreement, provided that the external toroidal vortices formed in the vicinity of the drops are ventilated by air blowing to avoid enrichment of the vortices with the liquid vapour.

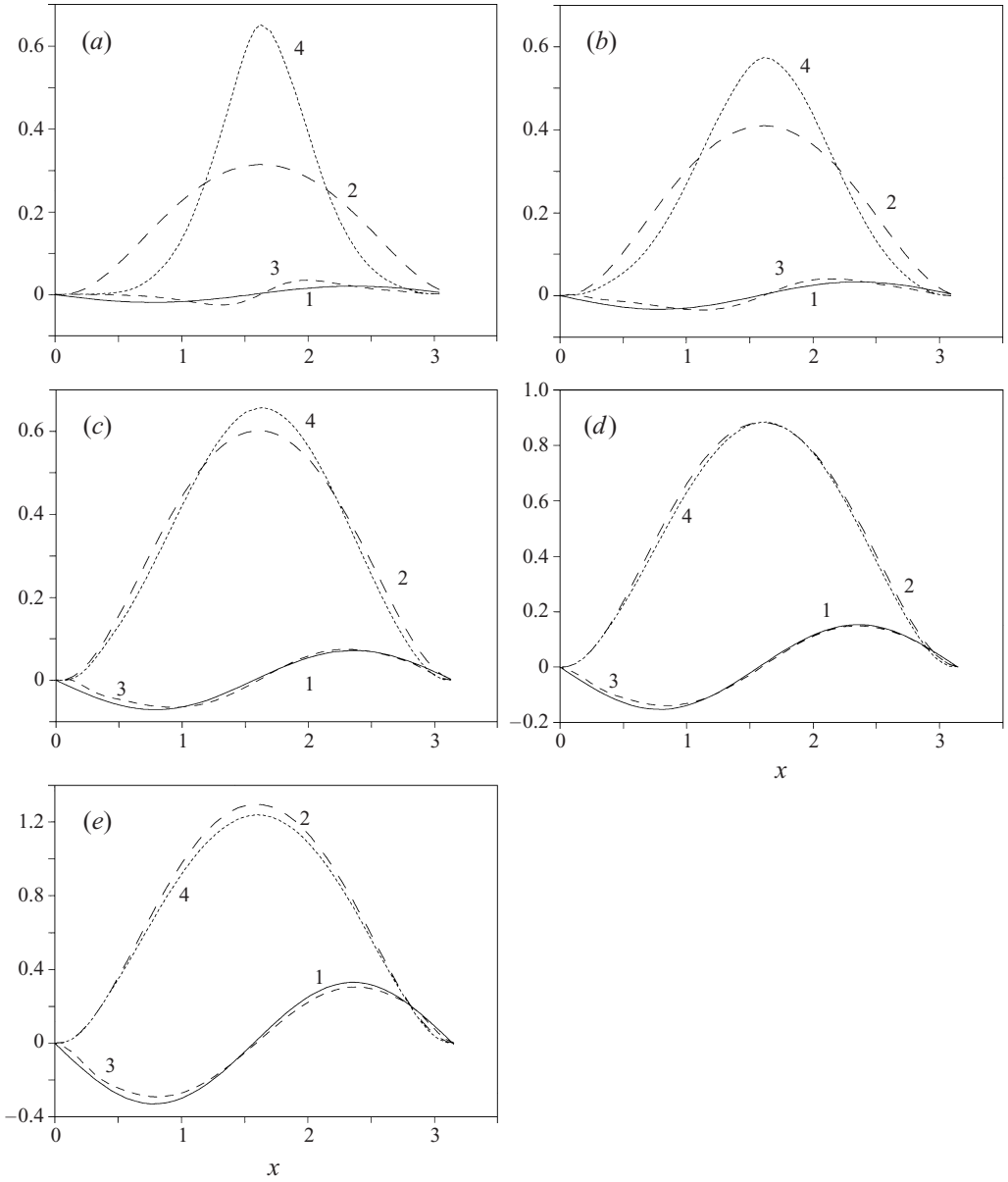

FIGURE 14. Distributions of the dimensionless acoustic streaming velocity $\langle \bar{u}_{1\infty} \rangle$ and the Sherwood number $\langle Sh \rangle$ over the droplet surface at $t = 0$. x is the dimensionless arclength of the droplet generatrix from the bottom O_1 (cf. figure 2*a*). SPL = 160.247 dB_e, n-hexadecane droplets. The analytical asymptotic results: curve 1, $\langle \bar{u}_{1\infty} \rangle$ given by (5.18); 2, $\langle Sh \rangle$ given by (7.3). The numerical results: 3, $\langle \bar{u}_{1\infty} \rangle$ given by (4.20); 4, $\langle Sh \rangle$ given by (6.34). The initial drop volumes are (*a*) 5 µl, (*b*) 1 µl, (*c*) 0.1 µl, (*d*) 0.01 µl, (*e*) 0.001 µl.

The authors wish to thank the Deutsche Forschungsgemeinschaft for the financial support of the present work by grant Br 1046/3-1 and -2. A. L. Y. is indebted to the Lehrstuhl für Strömungsmechanik at the Universität Erlangen-Nürnberg in Erlangen for partial financial assistance and for their hospitality in 1996 to 1998. This research was partially supported by GIF – German–Israeli Foundation for Scientific Research

and Development, Research Grant No. I-536-097.14/97, by the Elson/Shapiro Families Research Fund, by the Henri Gutwirth Fund for the Promotion of Research, and by the Fund for the Promotion of the Research at the Technion.

Appendix A

According to (4.10*a*) and (4.12) with $\eta \to \infty$

$$u_{0\infty} = A\cos\omega t + A_1 \sin\omega t, \tag{A 1a}$$

$$\begin{aligned} v_{0\infty} = -\Bigg\{ & \left(\frac{\mathrm{d}A}{\mathrm{d}x} + \frac{\mathrm{d}r/\mathrm{d}x}{r}A\right)\left(y\cos\omega t - \frac{\delta}{2}\cos\omega t - \frac{\delta}{2}\sin\omega t\right) \\ & + \left(\frac{\mathrm{d}A_1}{\mathrm{d}x} + \frac{\mathrm{d}r/\mathrm{d}x}{r}A_1\right)\left(y\sin\omega t - \frac{\delta}{2}\sin\omega t + \frac{\delta}{2}\cos\omega t\right) \\ & + y\frac{\omega}{c_0}B\left[-\left(\cos\frac{\omega z_1}{c_0} + p_{sr}\right)\sin\omega t + p_{si}\cos\omega t\right]\Bigg\}. \end{aligned} \tag{A 1b}$$

Accounting for (4.15) and (A 1) we obtain

$$\left\langle u_{0\infty}\int u_{0\infty}\,\mathrm{d}t\right\rangle = 0, \tag{A 2a}$$

$$\left\langle u_{0\infty}\int \frac{\partial u_{0\infty}}{\partial x}\,\mathrm{d}t\right\rangle = \frac{1}{2\omega}\left(-A\frac{\mathrm{d}A_1}{\mathrm{d}x} + A_1\frac{\mathrm{d}A}{\mathrm{d}x}\right), \tag{A 2b}$$

$$\begin{aligned} \left\langle u_{0\infty}\int v_{0\infty}\,\mathrm{d}t\right\rangle = -\frac{1}{2\omega}\Bigg\{ & A\left(\frac{\mathrm{d}A}{\mathrm{d}x} + \frac{\mathrm{d}r/\mathrm{d}x}{r}A\right)\frac{\delta}{2} \\ & + A_1\frac{\mathrm{d}A}{\mathrm{d}x}\left(y - \frac{\delta}{2}\right) + A\frac{\mathrm{d}A_1}{\mathrm{d}x}\left(-y + \frac{\delta}{2}\right) \\ & + A_1\left(\frac{\mathrm{d}A_1}{\mathrm{d}x} + \frac{\mathrm{d}r/\mathrm{d}x}{r}A_1\right)\frac{\delta}{2} \\ & + y\frac{\omega}{c_0}B\left[A\left(\cos\frac{\omega z_1}{c_0} + p_{sr}\right) + A_1 p_{si}\right]\Bigg\}, \end{aligned} \tag{A 2c}$$

$$\begin{aligned} \left\langle u_{0\infty}\int \frac{\partial v_{0\infty}}{\partial x}\,\mathrm{d}t\right\rangle = -\frac{1}{2\omega}\Bigg\{ & A\frac{\mathrm{d}}{\mathrm{d}x}\left(\frac{\mathrm{d}A}{\mathrm{d}x} + \frac{\mathrm{d}r/\mathrm{d}x}{r}A\right)\frac{\delta}{2} \\ & + \left[A_1\frac{\mathrm{d}}{\mathrm{d}x}\left(\frac{\mathrm{d}A}{\mathrm{d}x} + \frac{\mathrm{d}r/\mathrm{d}x}{r}A\right) - A\frac{\mathrm{d}}{\mathrm{d}x}\left(\frac{\mathrm{d}A_1}{\mathrm{d}x} + \frac{\mathrm{d}r/\mathrm{d}x}{r}A_1\right)\right] \\ & \times\left(y - \frac{\delta}{2}\right) + A_1\frac{\mathrm{d}}{\mathrm{d}x}\left(\frac{\mathrm{d}A_1}{\mathrm{d}x} + \frac{\mathrm{d}r/\mathrm{d}x}{r}A_1\right)\frac{\delta}{2} \\ & + y\frac{\omega}{c_0}B\left[A\frac{\partial}{\partial x}\left(\cos\frac{\omega z_1}{c_0} + p_{sr}\right) + A_1\frac{\partial p_{si}}{\partial x}\right]\Bigg\}, \end{aligned} \tag{A 2d}$$

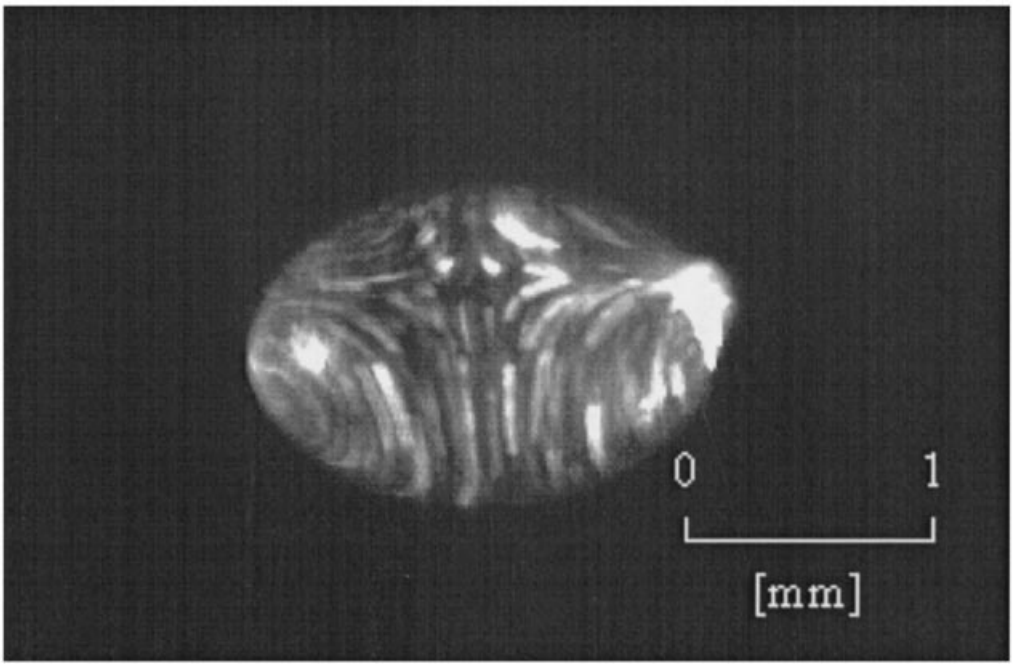

FIGURE 15. Visualized meridional section of the flow field inside a 2 μl methanol droplet with an aspect ratio $s_l/s_s = 1.5$. The streaks show two toroidal vortices which differ in size due to the levitation of the droplet below a pressure node. Flow velocities were measured using multi-exposure images with shorter exposure time.

$$\left\langle u_{0\infty} \int v_{0\infty}\, \mathrm{d}t \right\rangle = -\left\langle v_{0\infty} \int u_{0\infty}\, \mathrm{d}t \right\rangle, \quad \left\langle v_{0\infty} \int v_{0\infty}\, \mathrm{d}t \right\rangle = 0, \tag{A 2e, f}$$

$$\begin{aligned}\left\langle v_{0\infty} \int \frac{\partial v_{0\infty}}{\partial y}\, \mathrm{d}t \right\rangle = \frac{1}{2\omega} \Bigg\{ & -\frac{\delta}{2} \left[\left(\frac{\mathrm{d}A}{\mathrm{d}x} + \frac{\mathrm{d}r/\mathrm{d}x}{r} A \right)^2 + \left(\frac{\mathrm{d}A_1}{\mathrm{d}x} + \frac{\mathrm{d}r/\mathrm{d}x}{r} A_1 \right)^2 \right] \\ & + \frac{\omega B}{c_0} \frac{\delta}{2} \left[\left(\cos \frac{\omega z_1}{c_0} + p_{sr} \right) \right. \\ & \times \left(-\frac{\mathrm{d}A}{\mathrm{d}x} - \frac{\mathrm{d}r/\mathrm{d}x}{r} A + \frac{\mathrm{d}A_1}{\mathrm{d}x} + \frac{\mathrm{d}r/\mathrm{d}x}{r} A_1 \right) \\ & \left. - p_{si} \left(\frac{\mathrm{d}A}{\mathrm{d}x} + \frac{\mathrm{d}r/\mathrm{d}x}{r} A + \frac{\mathrm{d}A_1}{\mathrm{d}x} + \frac{\mathrm{d}r/\mathrm{d}x}{r} A_1 \right) \right] \Bigg\}. \end{aligned} \tag{A 2g}$$

Note also that from (A 2*c*) and (A 2*g*) it is seen that

$$\left\langle u_{0\infty} \int \frac{\partial v_{0\infty}}{\partial x}\, \mathrm{d}t \right\rangle \sim B \frac{B}{\omega a} \frac{\delta}{a}, \quad \left\langle v_{0\infty} \int \frac{\partial v_{0\infty}}{\partial y}\, \mathrm{d}t \right\rangle \sim B \frac{B}{\omega a} \frac{\delta}{a}. \tag{A 3a, b}$$

Appendix B

In this Appendix we consider an internal circulation in an acoustically levitated droplet and its possible effect on the acoustic streaming in gas. The liquid in the droplet

may be driven by the gas flow near its surface. In order to find a representative flow velocity inside the drop we carried out a simple experiment and thorough calculations. The calculations also reveal the influence of the liquid motion on the mass transfer in the gas.

Before starting the calculations we describe an experiment carried out to visualize the liquid motion in the droplet and to measure a typical circulation velocity in the liquid. Particle image velocimetry (PIV) was used as a measuring technique. A laser light sheet illuminating a meridional section of the droplet in the levitator was produced by a 100 mW Nd : YAG laser, using an arrangement of spherical and cylindrical lenses which provided a sheet thickness of about 100 μm. For visualizing the flow inside the droplet, small hollow glass spheres with a mean diameter of 2 μm were added to the droplet liquid as tracer particles. The laser light scattered by the particles was detected by a high-resolution high-speed CCD camera SENSICAM purchased from PCO Computer Optics Ltd. Figure 15 shows a result of this visualization experiment for a 2 μl methanol droplet with an aspect ratio $s_l/s_s = 1.5$. The streaks in the drop meridional section show clearly the structure of the flow inside the drop. It is seen that two toroidal vortices inside the droplet set in. The vortices differ from each other in size, since the droplet is levitated below a pressure node. The measurement of a typical flow velocity inside the droplet was carried out using four exposures on one image frame, each with an exposure time of 100 μs, and a time delay of 1000 μs between the exposures. The flow velocity was calculated from these images using the auto-correlation technique. A PIV experiment was carried out using a 2 μl methanol droplet at an aspect ratio $s_l/s_s = 1.14$ (i.e. different from the droplet visualized in figure 15), corresponding to an SPL of 159.997 $\mathrm{dB_e}$. The velocity measured at a position close to the drop surface in the equator plane of this drop was 2.4 $\mathrm{cm\,s^{-1}}$.

In order to find the liquid motion theoretically, use should be made of the conditions that at the gas/liquid interface the velocity and shear stresses are continuous. In the leading order $O(B)$ these conditions replace the boundary condition (4.8*b*) and allow one to calculate both the gas and liquid motions solving the conjugate problem. In the leading order the Stokes layer should also appear in the liquid near the droplet surface. Thus, the condition of continuity of the shear stresses yields the estimate

$$\mu_l \frac{u_{l0}}{\left(\nu_l/\omega\right)^{1/2}} \sim \mu_0 \frac{B}{\left(\nu_0/\omega\right)^{1/2}}, \tag{B 1}$$

where μ_l and ν_l are the dynamic and kinematic viscosities of the liquid, and u_{l0} is the magnitude of the liquid velocity at the interface in the leading order.

According to (B 1), $u_{l0} = \chi B$, where $\chi = (\mu_0\rho_0/\mu_l\rho_l)^{1/2}$. Virtually for all liquids $\chi \leqslant 10^{-5/2} \ll 1$. Since $u_{l0} \ll B$, application of the no-slip condition in the form of (4.8*b*) in the leading order is justified. The corresponding Reynolds stresses in the droplet are $O(\chi^2)$ and may be neglected, which means that the liquid's own 'drive' for the steady liquid streaming is weak and negligible.

However, a steady circulation within the droplet may also result from liquid entrainment at the interface by the steady acoustic streaming in the gas. This circulation will envelope the whole body of the droplet (not only a thin Stokes layer near its surface). An estimate of the velocity magnitude u_{l1} in such a circulation can be readily obtained from the continuity of the shear stresses at the droplet surface as

$$\mu_l \frac{u_{l1}}{a} \sim \mu_0 \frac{B_s}{\left(\nu_0/\omega\right)^{1/2}}, \tag{B 2}$$

where $B_s = B^2/\omega a$ is the magnitude of the acoustic streaming velocity in gas (given e.g. by (5.19)).

The estimate yields

$$u_{l1} \sim \left[\frac{a}{\mu_l}\sqrt{\mu_0\rho_0\omega}\right] B_s. \tag{B 3}$$

For $a \sim 10^{-1}$ cm, $\mu_0 \sim 10^{-4}\,\mathrm{g\,cm^{-1}\,s^{-1}}$, $\rho_0 \sim 10^{-3}\mathrm{g\,cm^{-3}}$, $\omega = 56 \times 2\pi \times 10^3\,\mathrm{s^{-1}}$, and $\mu_l \sim 10^{-2}\mathrm{g\,cm^{-1}\,s^{-1}}$ one obtains $u_{l1} \sim 1.88 B_s$, which shows that the estimate (definitely yielding the correct scaling) is, nevertheless, quite inaccurate, since a dimensionless factor missing in it may be significantly smaller than 1. We shall, indeed, find that this is the case in the detailed calculation below.

First of all, let us find the shear stress acting at the droplet surface from the acoustic streaming flow. It is emphasized that we now disregard the boundary condition (4.14) at $y = 0$, which is replaced by the conditions of continuity of the velocity and shear stresses at the droplet surface. Integrating equation (4.16) using (3.5), (4.10*a*), and (4.12) as well as the boundary condition (4.14) for $y = \infty$, we find the derivative $\partial\langle u_1\rangle/\partial\eta$. At $\eta = 0$ we obtain

$$\begin{aligned}\left.\frac{\partial\langle u_1\rangle}{\partial\eta}\right|_{\eta=0} = &-\frac{1}{\omega}\left(A\frac{\mathrm{d}A}{\mathrm{d}x} + A_1\frac{\mathrm{d}A_1}{\mathrm{d}x}\right)\left(-\frac{1}{2}\right) - \frac{1}{\omega}\left(A\frac{\mathrm{d}A_1}{\mathrm{d}x} - A_1\frac{\mathrm{d}A}{\mathrm{d}x}\right)\left(-\frac{1}{2}\right)\\ &+\frac{B}{c_0}\left\{A\left[-\frac{1}{2}\left(\cos\frac{\omega(z+L)}{c_0} + p_{sr}\right)\right] + A_1\left[-\frac{1}{2}\left(\cos\frac{\omega(z+L)}{c_0} + p_{sr}\right)\right]\right.\\ &\left.+ Ap_{si}\frac{1}{2} + A_1 p_{si}\left(-\frac{1}{2}\right)\right\} + [n(\gamma-1)-1]\frac{B}{c_0}\left\{-Ap_{si}\left(-\frac{1}{2}\right) + A\left(-\frac{1}{2}\right)\right.\\ &\left.\times\left[\cos\frac{\omega(z+L)}{c_0} + p_{sr}\right] + A_1\left(-\frac{1}{2}\right)\left[\cos\frac{\omega(z+L)}{c_0} + p_{sr}\right] + A_1 p_{si}\left(-\frac{1}{2}\right)\right\}.\end{aligned} \tag{B 4}$$

From now on we consider an incompressible limit corresponding to the case of a small spherical droplet (cf. § 5). We assume that it sustains its spherical shape due to the surface tension in spite of the forces from the gas side, which is actually similar to the assumption used in Taylor (1932) to calculate the viscosity of emulsions. Accounting for (5.2), (5.3), (5.8), (5.14), (5.17), and the fact that $\Omega^2 \ll 1$, we reduce (B 4) to

$$\left.\frac{\partial\langle u_1\rangle}{\partial\eta}\right|_{\eta=0} = \frac{9}{8}\frac{B^2}{\omega a}\sin\theta\cos\theta, \tag{B 5}$$

where θ, as in § 5, is the angle reckoned from the droplet bottom (cf. figure 1).

Therefore the shear stress imposed by the acoustic streaming flow on the droplet surface is given by

$$\sigma_{R\theta}|_{R=a} = \mu_0\left.\frac{\partial\langle u_1\rangle}{\partial y}\right|_{y=0} = \sqrt{\rho_0\mu_0\omega}\,\frac{9}{16\sqrt{2}}\frac{B^2}{\omega a}\sin 2\theta, \tag{B 6}$$

where $\sigma_{R\theta}|_{R=a}$ is the shear stress in the liquid.

Expression (4.17) for the acoustic streaming in gas holds. However, the constant of integration C in it is now found using the velocity continuity at the droplet surface

$$\langle u_1\rangle|_{\eta=0} = v_\theta|_{R=a}, \tag{B 7}$$

where $v_\theta|_{R=a}$ is the liquid velocity at the surface which is found below.

Using (B 7), we arrive at (4.18) and (4.20) with an additional term $v_\theta|_{R=a}$ on the right. As a result, for the small spherical droplet we are dealing with here, we obtain

$$\langle u_{1\infty}\rangle = v_\theta|_{R=a} - \frac{45}{32}\frac{B^2}{\omega a}\sin 2\theta \tag{B 8}$$

which replaces (5.18).

We now proceed towards calculation of the internal circulation in the droplet subject to the boundary condition (B 6). For a droplet of radius $a = 10^{-2}$ cm, given the velocity magnitude of the internal circulation of the order of $B_s \sim 1\,\mathrm{cm\,s^{-1}}$ and the kinematic viscosity $\nu_l \sim 10^{-2}\,\mathrm{cm^2\,s^{-1}}$, we estimate the Reynolds number $Re_l = B_s a/\nu_l \sim 1$, which permits use of the Stokes equations for the internal flow. This approximation certainly will be less accurate for $a \sim 10^{-1}$ cm ($Re_l \sim 10$). However, even in this case the inertial effects will still be not too large, and the extrapolation of the result may lead to a plausible estimate. We use the general solution of the Stokes equations in spherical harmonics given in Lamb (1959, §§ 335 and 336). We adopt in the rest of this Appendix the notation of Lamb (1959) which is different from (and should not be mixed with) the other parts of the present paper. We denote the Cartesian coordinate system x, y and z with the origin at the droplet centre, and x being reckoned from the centre towards the droplet bottom (parallel and opposite to z of figure 1). The corresponding Cartesian components of the liquid velocity $\mathbf{v}$ are denoted u, v and w. We also introduce the spherical coordinate system R, θ (the same R and θ as in § 5; also cf. figure 1), and φ with the origin at the droplet centre, which yields

$$x = R\cos\theta, \quad y = R\sin\theta\cos\varphi, \quad z = R\sin\theta\sin\varphi. \tag{B 9}$$

Since the unity vector of the angular direction θ, $\boldsymbol{e}_\theta$ is given by

$$\boldsymbol{e}_\theta = -\boldsymbol{i}\sin\theta + \boldsymbol{j}\cos\theta\cos\varphi + \boldsymbol{k}\cos\theta\sin\varphi, \tag{B 10}$$

we obtain

$$\sigma_{R\theta} = \boldsymbol{\sigma}_R \cdot \boldsymbol{e}_\theta = -\sin\theta\ \sigma_{Rx} + \cos\theta\cos\varphi\ \sigma_{Ry} + \cos\theta\sin\varphi\ \sigma_{Rz}, \tag{B 11a}$$

$$v_\theta = \boldsymbol{v} \cdot \boldsymbol{e}_\theta = -\sin\theta\ u + \cos\theta\cos\varphi\ v + \cos\theta\sin\varphi\ w. \tag{B 11b}$$

The liquid velocity at the droplet surface is that of the acoustic streaming on the gas side, and thus the only non-zero component of $\boldsymbol{v}|_{R=a}$ on the liquid side is v_θ, and the only non-zero component of $(\mathrm{curl}\,\boldsymbol{v})|_{R=a}$ is $(\mathrm{curl}\,\boldsymbol{v})_\theta$. The expressions for $\boldsymbol{R}\cdot\mathrm{curl}\,\boldsymbol{v}$ and $\boldsymbol{R}\cdot\boldsymbol{v}$ following from Lamb's solution are

$$\boldsymbol{R}\cdot\mathrm{curl}\,\boldsymbol{v} = \sum_{n=-\infty}^{\infty} n(n+1)\,\chi_n, \tag{B 12a}$$

$$\boldsymbol{R}\cdot\boldsymbol{v} = \frac{1}{\mu_l}\sum_{n=-\infty}^{\infty}\frac{nR^2}{2(2n+3)}p_n + \sum_{n=-\infty}^{\infty} n\varphi_n \tag{B 12b}$$

with $\boldsymbol{R}$ being the radius vector from the droplet centre, p_n a solid harmonic of degree n, and φ_n and χ_n arbitrary harmonics of degree n.

Taking (B 12) at the droplet surface $R = a$ and accounting for the fact that $\boldsymbol{R}$ is aligned in the radial direction, whereas both $\mathrm{curl}\,\boldsymbol{v}$ and $\boldsymbol{v}$ point in the angular direction (θ), we find that $\mathbf{R}\cdot\mathrm{curl}\,\boldsymbol{v} = 0$ and $\mathbf{R}\cdot\boldsymbol{v} = 0$ at the droplet surface, and thus

from (B 12) we obtain

$$\chi_n \equiv 0, \quad \frac{1}{\mu_l}\sum_{n=-\infty}^{\infty}\frac{na^2}{2(2n+3)}p_n + \sum_{n=-\infty}^{\infty} n\varphi_n = 0. \tag{B 13a, b}$$

Using the general solution of the Stokes equations in spherical harmonics from Lamb (1959) and accounting for (B 11) and (*B* 13*a*), we obtain the expressions for the shear stress and the angular velocity at the droplet surface in the form

$$\begin{aligned}\sigma_{R\theta}|_{R=a} = \sum_{n=-\infty}^{\infty}\Bigg\{&\frac{n-1}{2n+1}\,a\,\left(-\sin\theta\frac{\partial p_n}{\partial x}+\cos\theta\cos\varphi\frac{\partial p_n}{\partial y}+\cos\theta\sin\varphi\frac{\partial p_n}{\partial z}\right)\\&+\frac{(2n^2+4n+3)}{(n+1)(2n+1)(2n+3)}a^{2n+2}\left[-\sin\theta\frac{\partial}{\partial x}\left(\frac{p_n}{R^{2n+1}}\right)\right.\\&\left.+\cos\theta\cos\varphi\frac{\partial}{\partial y}\left(\frac{p_n}{R^{2n+1}}\right)+\cos\theta\sin\varphi\frac{\partial}{\partial z}\left(\frac{p_n}{R^{2n+1}}\right)\right]\Bigg\}\\&+\frac{2\mu_l}{a}\sum_{n=-\infty}^{\infty}(n-1)\left(-\sin\theta\frac{\partial\varphi_n}{\partial x}+\cos\theta\cos\varphi\frac{\partial\varphi_n}{\partial y}+\cos\theta\sin\varphi\frac{\partial\varphi_n}{\partial z}\right),\end{aligned} \tag{B 14a}$$

$$\begin{aligned}v_\theta|_{r=a} = \frac{1}{\mu_l}\sum_{n=-\infty}^{\infty}\Bigg\{&\frac{a^2}{2(2n+1)}\left(-\sin\theta\frac{\partial p_n}{\partial x}+\cos\theta\cos\varphi\frac{\partial p_n}{\partial y}\right.\\&\left.+\cos\theta\sin\varphi\frac{\partial p_n}{\partial z}\right)+\frac{na^{2n+3}}{(n+1)(2n+1)(2n+3)}\left[-\sin\theta\frac{\partial}{\partial x}\left(\frac{p_n}{R^{2n+1}}\right)\right.\\&\left.+\cos\theta\cos\varphi\frac{\partial}{\partial y}\left(\frac{p_n}{R^{2n+1}}\right)+\cos\theta\sin\varphi\frac{\partial}{\partial z}\left(\frac{p_n}{R^{2n+1}}\right)\right]\Bigg\}\\&+\sum_{n=-\infty}^{\infty}\left(-\sin\theta\frac{\partial\varphi_n}{\partial x}+\cos\theta\cos\varphi\frac{\partial\varphi_n}{\partial y}+\cos\theta\sin\varphi\frac{\partial\varphi_n}{\partial z}\right).\end{aligned} \tag{B 14b}$$

Note that on the right-hand sides of (B 14) $R = a$ should be substituted after the differentiation.

Given the boundary condition imposed on $\sigma_{R\theta}|_{R=a}$ (cf. (B 6)) and (B 9), it is easy to see that the only two spherical harmonics needed in the present case are

$$p_2 = E'R^2\tfrac{1}{2}\left(3\cos^2\theta - 1\right) = E'\tfrac{1}{2}\left(3x^2 - R^2\right), \tag{B 15a}$$

$$\varphi_2 = E''R^2\tfrac{1}{2}\left(3\cos^2\theta - 1\right) = E''\tfrac{1}{2}\left(3x^2 - R^2\right), \tag{B 15b}$$

with all the other harmonics being zero.

Substituting (B 15) in (B 14*a*), we find

$$\sigma_{R\theta}|_{R=a} = \left(-\tfrac{4}{7}a^2E' - 3\mu_lE''\right)\sin 2\theta. \tag{B 16}$$

Therefore the boundary condition (B 6) together with (B 16) yields

$$\sqrt{\rho_0\mu_0\omega}\,\frac{9}{16\sqrt{2}}\,\frac{B^2}{\omega a} = -\tfrac{4}{7}a^2E' - 3\mu_lE''. \tag{B 17}$$

Substituting (B 15) in (*B* 13*b*), we find additionally

$$E'' = -\frac{E'a^2}{14\mu_l}. \tag{B 18}$$

Solving the system (B 17) and (B 18), we find E' and E'' as

$$E' = -\frac{14}{5}\frac{1}{a^2}\sqrt{\rho_0\mu_0\omega}\,\frac{9}{16\sqrt{2}}\frac{B^2}{\omega a}, \qquad E'' = \frac{1}{5\mu_l}\sqrt{\rho_0\mu_0\omega}\,\frac{9}{16\sqrt{2}}\frac{B^2}{\omega a}. \tag{B 19a,b}$$

Substituting (B 15) and (B 19) into (B 14*b*), we find

$$v_\theta|_{R=a} = \frac{9}{80\sqrt{2}}\left(\frac{a}{\mu_l}\sqrt{\rho_0\mu_0\omega}\right)\frac{B^2}{\omega a}\sin 2\theta \tag{B 20}$$

which improves the rough estimate of (B 3).

The general solution of the Stokes equations given in Lamb (1959) with the harmonics of (B 15) yields after a simple rearrangement and the use of (B 18) the whole flow field inside the acoustically levitated droplet

$$v_R = \frac{E'}{14\mu_l}\left(2\cos^2\theta - \sin^2\theta\right)\left(R^3 - a^2R\right), \quad v_\theta = \frac{E'}{28\mu_l}\sin 2\theta\left(3a^2R - 5R^3\right). \tag{B 21a,b}$$

Introducing the stream function Ψ by the relations

$$\frac{\partial\Psi}{\partial R} = -v_\theta R\sin\theta, \quad \frac{\partial\Psi}{\partial\theta} = v_R R^2\sin\theta, \tag{B 22}$$

and using (B 21), we find

$$\Psi = \frac{E'a^5}{28\mu_l}\sin\theta\sin 2\theta\left[\left(\frac{R}{a}\right)^5 - \left(\frac{R}{a}\right)^3\right], \tag{B 23}$$

where E' is given by (B 19*a*).

It is emphasized that a similar flow inside a droplet was predicted by Taylor (1966) in his work on the circulation produced in a drop by an electric field. There the tangential stress imposed by the electric field on the droplet surface has the same angular dependence as that of (B 6) resulting from the acoustic streaming. Therefore the stream function given by (16) and (18) in Taylor (1966) is essentially the same as that of (B 23) (except the constant factor $E'a^5/28\mu_l$). Consequently the streamlines depicted in figure 1 of Taylor (1966), as well as the circulation seen in the photograph of his figure 2 represent (up to a constant factor) the structure of the flow inside an acoustically levitated droplet. Also the photograph shown in figure 15 of the present work is reminiscent of figure 2 of Taylor (1966), and also the flow field (B 23) closely corresponds to the flow field recorded in the present work in figure 15. There is an important difference, however, in the steady motion of the medium outside the droplet. In the situation studied by Taylor (1966) the flow outside the droplet does not form a boundary layer similar to the acoustic one, and is always in the same direction as the droplet liquid flow at the interface (e.g. see his figure 1). In our case, however, the situation is more complicated. Indeed, according to (B 8) and (B 20), the acoustic streaming velocity in the gas at the outer boundary of the acoustic boundary layer becomes

$$\langle u_{1\infty}\rangle = \frac{9}{80\sqrt{2}}\left(\frac{a}{\mu_l}\sqrt{\rho_0\mu_0\omega}\right)\frac{B^2}{\omega a}\sin 2\theta - \frac{45}{32}\frac{B^2}{\omega a}\sin 2\theta. \tag{B 24}$$

It is seen that according to (B 24) the liquid flow reduces the acoustic streaming velocity $\langle u_{1\infty}\rangle$. This results from the fact that the gas flow at the liquid interface is opposite to that at the outer boundary of the acoustic boundary layer (cf. figure 3). This situation is completely different from that considered in Taylor (1966).

It is instructive to compare the magnitude of the first term on the right in (B 24), $v_\theta|_{R=a}$, to the second one, $\langle u_{1\infty}\rangle_0$, to estimate the effect of the circulation in the liquid on the acoustic streaming flow in gas. Their ratio is

$$\frac{|v_\theta|_{R=a}|}{|\langle u_{1\infty}\rangle_0|} = \frac{\sqrt{2}}{25}\left(\frac{a}{\mu_l}\sqrt{\rho_0\mu_0\omega}\right). \tag{B 25}$$

Taking $\rho_0 \sim 10^{-3}\,\mathrm{g\,cm^{-3}}$, $\mu_0 \sim 10^{-4}\,\mathrm{g\,cm^{-1}\,s^{-1}}$, $\mu_l \sim 10^{-2}\,\mathrm{g\,cm^{-1}\,s^{-1}}$, $\omega = 56 \times 2\pi \times 10^3\,\mathrm{s^{-1}}$, and $a \sim 10^{-2}\,\mathrm{cm}$, we find from (B 25) the ratio of 0.0106. Extrapolating to much larger droplets with $a \sim 10^{-1}\,\mathrm{cm}$, we obtain the ratio of 0.106. Therefore in the worst case the effect of the circulation in the liquid on the acoustic streaming velocity at the outer boundary of the acoustic boundary layer is about 10%. If this effect were incorporated in the calculation of the mass flux from the droplet surface during its evaporation in a strong acoustic field, it would actually modify only the expression for $\langle \tilde{u}_{1\infty}\rangle$ in (6.24*b*) with all the other formulae being the same. Thus, according to (9.17) with V_c of the order of the acoustic streaming velocity at the outer boundary of the acoustic boundary layer, one expects the Sherwood number value to increase by a factor of about $(1.1)^{1/2} = 1.049$. This factor is close to 1, which allows us to neglect the effect of the internal circulation of liquid within the droplet on the acoustic streaming velocity and the mass transfer rate, as has been done throughout the main body of the paper.

In the case of heat removal from a warm droplet a possible slightly non-uniform temperature distribution in the liquid may also result in a surface-tension-driven circulation. For a temperature difference of the order of $10^{-1}\,^\circ\mathrm{C}$ we find from (8.5) and table 1 a surface tension variation of the order of $\Delta\alpha = 10^{-2}\,\mathrm{g\,s^{-2}}$. This results in the shear stress of the order of $\mu_l u_l/a \sim \Delta\alpha/(2\pi a)$. Given $\mu_l \sim 10^{-2}\,\mathrm{g\,cm^{-1}\,s^{-1}}$, we estimate $u_l \sim 10^{-1}\,\mathrm{cm\,s^{-1}}$ due to the Marangoni convection, which certainly could be neglected. For a temperature difference of the order of $1\,^\circ\mathrm{C}$, we obtain an estimate $u_l \sim 1\,\mathrm{cm\,s^{-1}}$. The mixing time, however, becomes very short, of the order of $2\pi a/u_l \leqslant 0.6\,\mathrm{s}$ for $a \leqslant 10^{-1}\,\mathrm{cm}$. Therefore in the process with the duration of the order of 10^2 to $10^3\,\mathrm{s}$ we are dealing with, the Marangoni mixing will tend to reduce the temperature difference, and thus u_l, to a level, where the latter can be safely neglected.

REFERENCES

Andrade, E. N. 1931 On the circulation caused by the vibration of air in a tube. *Proc. R. Soc. Lond.* A **134**, 447.

Bird, R. B., Stewart, W. E. & Lightfoot, E. N. 1960 *Transport Phenomena.* John Wiley.

Burdukov, A. P. & Nakoryakov, V. E. 1965*a* Heat transfer from a cylinder in a sound field at Grashof numbers approaching zero. *J. Appl. Mech. Tech. Phys.* **6** No. 1, 112.

Burdukov, A. P. & Nakoryakov, V. E. 1965*b* On mass transfer in an acoustic field. *J. Appl. Mech. Tech. Phys.* **6** No. 2, 51.

Burdukov, A. P. & Nakoryakov, V. E. 1967 Effects of vibrations on mass transfer from a sphere at high Prandtl numbers. *J. Appl. Mech. Tech. Phys.* **8** No. 3, 111.

Fuller, E. N., Schettler, P. D. & Giddings, J. C. 1966 A new method for prediction of binary gas-phase diffusion coefficients. *Indust. Engng Chem.* **58**, 18. See also *VDI Wärmeatlas*, 6th Edn. (1991).

Gopinath, A. & Mills, A. F. 1993 Convective heat transfer from a sphere due to acoustic streaming. *Trans. ASME: J. Heat Transfer* **115**, 333.

Hildebrand, F. B. 1974 *Introduction to Numerical Analysis*. Dover.

Krasilnikov, V. A. & Krylov, V. V. 1984 *Introduction into Physical Acoustics*. Nauka (in Russian).

Lamb, H. 1959 *Hydrodynamics*, 6th Edn. Cambridge University Press.

Landau, L. D. & Lifshitz, E. M. 1959 *Fluid Mechanics*. Pergamon.

Larsen, P. S. & Jensen, J. W. 1978 Evaporation rates of drops in forced convection with superposed transverse sound field. *Intl J. Heat Mass Transfer* **21**, 511.

Lee, C. P. & Wang, T. G. 1988 Acoustic radiation force on a heated sphere including effects of heat transfer and acoustic streaming. *J. Acoust. Soc. Am.* **83**, 1324.

Lee, C. P. & Wang, T. G. 1989 Near-boundary streaming around a small sphere due to orthogonal standing waves. *J. Acoust. Soc. Am.* **85**, 1081.

Lee, C. P. & Wang, T. G. 1990 Outer acoustic streaming. *J. Acoust. Soc. Am.* **88**, 2367.

Leung, E. W. & Wang, T. G. 1985 Force on a heated sphere in a horizontal plane acoustic standing wave. *J. Acoust. Soc. Am.* **77**, 1686.

Lighthill, M. J. 1954 The response of laminar skin friction and heat transfer to fluctuations in the stream velocity. *Proc. R. Soc. Lond.* A **224**, 1.

Maisel, B. S. & Sherwood, T. K. 1950 Evaporation of liquids into turbulent gas streams. *Chem. Engng Progr.* **46**, 131.

Ranz, W. E. & Marshall, W. R. 1952*a* Evaporation from drops. Part I. *Chem. Engng Progr.* **48**, 141.

Ranz, W. E. & Marshall, W. R. 1952*b* Evaporation from drops. Part II. *Chem. Engng Progr.* **48**, 173.

Rayleigh, Lord 1883 On the circulation of air observed in Kundt's tubes and on some allied acoustical problems. *Phil. Trans. R. Soc. Lond.* **175**, 1.

Reid, R. C., Prausnitz, J. M. & Poling, B. E. 1987 *The Properties of Gases and Liquids*. McGraw-Hill.

Riley, N. 1966 On a sphere oscillating in a viscous fluid. *Q. J. Mech. Appl. Maths* **19**, 461.

Riley, N. 1997 Acoustic streaming. In *Encyclopedia of Acoustics* (ed. M. J. Crocker), vol. 1, p. 321. Wiley.

Richardson, P. D. 1967 Heat transfer from a circular cylinder by acoustic streaming. *J. Fluid Mech.* **30**, 337.

Schlichting, H. 1932 Berechnung ebener periodischer Grenzschichtströmungen. *Phys. Z.* **33**, 327.

Schlichting, H. 1979 *Boundary Layer Theory*. McGraw-Hill.

Seaver, M., Galloway, A. & Manuccia, T. J. 1989 Acoustic levitation in a free-jet wind tunnel. *Rev. Sci. Instrum.* **60**, 3452.

Seaver, M. & Peele, J. R. 1990 Noncontact fluorescence thermometry of acoustically levitated water drops. *Appl. Optics* **29**, 1956.

Shi, T. & Apfel, R. E. 1995 Oscillations of a deformed liquid drop in an acoustic field. *Phys. Fluids* **7**, 1545.

Stuart, J. T. 1966 Double boundary layers in oscillatory viscous flow. *J. Fluid Mech.* **24**, 673.

Taylor, G. I. 1932 The viscosity of a fluid containing small drops of another fluid. *Proc. R. Soc. Lond.* A **138**, 41. Reprinted in *The Scientific Papers of Sir G. I. Taylor*, vol. IV, N10. Cambridge University Press, 1971.

Taylor, G. I. 1966 The circulation produced in a drop by an electric field. *Proc. R. Soc. Lond.* A **291**, 159. Reprinted in *The Scientific Papers of Sir G. I. Taylor*, vol. IV, N43. Cambridge University Press, 1971.

Tian, Y. & Apfel, R. E. 1996 A novel multiple drop levitator for the study of drop arrays. *J. Aerosol Sci.* **27**, 721.

Trinh, E. H. & Hsu, C.-J. 1986 Equilibrium shapes of acoustically levitated drops. *J. Acoust. Soc. Am.* **79**, 1335.

Trinh, E. H. & Robey, J. L. 1994 Experimental study of streaming flows associated with ultrasonic levitators. *Phys. Fluids* **6**, 3567.

Yarin, A. L., Brenn, G., Keller, J., Pfaffenlehner, M., Ryssel, E. & Tropea, C. 1997 Flowfield characteristics of an aerodynamic/acoustic levitator. *Phys. Fluids* **9**, 3300.

Yarin, A. L., Pfaffenlehner, M. & Tropea, C. 1998 On the acoustic levitation of droplets. *J. Fluid Mech.* **356**, 65 (referred to herein as YPT).

Zevenbergen, J. F., Dahoe, A. E., Pekalski, A. A., Ruiter, B. R. de & Scarlett, B. 1998 Laser ignition of single magnesium particles. In *Ninth Intl Symp. on Applications of Laser Techniques to Fluid Mechanics, Lisbon, Portugal, July 13–16*, vol. II, p. 35.6.1.